STUDY OF EQUILIBRIUM AIR TOTAL RADIATION

Final Report

Contract No. NASw-939 and -1303

September 1968

Prepared for

NATIONAL AERONAUTICS AND SPACE ADMINISTRATION

Office of Advanced Research and Technology

Washington, D. C.

CONTENTS

CONTENTS

LIST OF FIGURES

PAGE

iii

LIST OF FIGURES

LIST OF FIGURES

v

LIST OF FIGURES

NOMENCLATURE

A	=	area
D	=	diameter
E_D	=	driver energy density
F_H	=	enthalpy flux
H	=	altitude
I	=	intensity
L	=	gas layer thickness
L_D	=	driver length
F, p	=	pressure
Q	=	heat transfer rate
Q_{NOM}	=	energy of capacitor bank
R	=	electrical resistance
R_N	=	nose radius
T	=	temperature
U, u	=	velocity
V	=	voltage, volume
W	=	weight of the vehicle
c	=	specific heat
h	=	enthalpy, Flanck's constant
i	=	current
k	=	coefficient of thermal conductivity, Boltzmann constant
q_r	=	radiative heat flux
q_{r_c}	=	coupled radiative heat flux
q_{r_u}	=	uncoupled radiative heat flux
r	=	polar coordinate
t	=	time
x	=	distance
Γ	=	coupling parameter
Ω	=	solid angle
α	=	thermal coefficient of resistance
γ_e	=	entry angle from horizontal
$\underline{\epsilon_\nu}$	=	spectral emission coefficient
ϵ	=	emissivity, Eq. (2.17)
$\varkappa_\nu$	=	spectral absorption coefficient
λ	=	wavelength, dummy variable
ν	=	frequency
ρ	=	density
σ	=	Stefan-Boltzmann constant

Subscripts

e	=	entry conditions
f	=	flight
m	=	model
i	=	ith element
s	=	stagnation conditions (also shock)
o	=	initial, also standard
1	=	initial driven tube conditions
∞	=	free stream

FOREWORD

This document contains results obtained during the study supported by the Office of Advanced Research and Technology under Contracts NASw - 939 and - 1303.

The work was performed in the Experimental Fluid Physics Section - Dr. W. R. Warren, Manager - of the Space Sciences Laboratory (SSL), General Electric Company.

The principal investigator was J. S. Gruszczynski. He was supported by a team of specialists and technicians.

ACKNOWLEDGMENTS

1. INTRODUCTION

1.1 Discussion of the Problem

The problem of radiative heat transfer to the surface of a space vehicle during entry into a planetary atmosphere has gained in importance with the establishment of national programs for lunar exploration and missions to the near planets. The entry velocities for some of these missions will be well above the Earth orbital value and, therefore, the flow in the stagnation region of a blunt vehicle will reach high pressure and temperature levels. Such gas can be expected to emit large amounts of radiant energy with intensities and spectral distributions characteristic of the chemical species present in the flow. To illustrate the property levels of interest, we have shown in Fig. 1.1 an altitude-velocity map for Earth re-entry on which lines of constant blunt body stagnation density, temperature and ion mole fraction (assuming equilibrium thermochemistry) are drawn. Two hypothetical vehicle trajectories are also shown. It can be seen that equilibrium stagnation temperatures of more than $14,000^{\rm o}$ K and relatively high degree of ionization will be reached for the re-entry from a Mars mission. At these conditions the heat transfer problem ceases to be only one of convection across the boundary layer. The radiative energy emitted by the gas in the shock layer will be absorbed by the surface of the vehicle adding to the total heat transfer. At sufficiently high entry velocities this mode of heat transfer will eventually dominate the overall aerodynamic heating.

In considering the contribution of radiative transport processes to the heat transfer experienced by an entry vehicle, a distinction is made between equilibrium radiation originating in the shock-processed gas, which after passing through the bow wave has relaxed to its state of thermochemical equilibrium, and the non-equilibrium radiation, which is emitted from the shock front in which the imparted energy has not been distributed among the various available degrees of freedom. The relative contributions of these processes depend mainly on the flight altitude (ambient gas density) and to a lesser degree on the flight velocity.

The radiance of high temperature air is a result of several complex physical processes and, although the fundamentals have been studied theoretically in detail, its prediction depends to a considerable extent on many approximating assumptions. Therefore, experimental data are required to evaluate the predictions.

Thermal radiation from entry body flow fields has been investigated extensively for many years. Early studies were largely concerned with orbital and sub-orbital Earth entry. With the increased interest in superorbital entry velocities, many recent theoretical studies and laboratory and flight experiments have been concentrated in this regime. Through a simplified analysis of the radiative recombination atomic deionization and free-free transition mechanisms, Breene [1] [2] and his associates predicted that for temperature and density levels associated

-2-

with a hypervelocity entry a large fraction of the energy radiated from a thin layer of gas (a 1 cm layer thickness was generally assumed) would be at wavelengths below 0.2μ. This was further confirmed analytically by Biberman (3) (4) and his associates who have published theoretical results for high temperature air that showed the importance of the vacuum UV spectral region. This work also concluded that the deionization and free-free (brehmstrahlung) mechanisms were important and also that atomic lines radiation would be a strong contributor to high temperature gas radiance over important ranges of temperature, density and gas layer thickness.

To illustrate this we are showing in Fig. 1.2 two theoretical spectral distributions of air radiance, one for air at 7000°K and 1 atm (1) and the other at 14000°K and the same pressure without the contribution of spectral lines (3). The spectrum at the lower temperature contains mostly emission from molecular bands in the UV, visible and IR range. Very little emission is expected below 1800 $\overset{o}{A}$ due to the limitation of blackbody radiation. At the higher temperature, however, the free-bound transitions in the vacuum UV part of the spectrum are very pronounced. Several other contributions to the theoretical aspects of this problem have been made; for example, see Refs. 5 - 11.

1.2 Experimental Approach

The study of radiative properties of high temperature gases is confronted with the problem of producing uniform samples of the gas at approximately

constant temperature and pressure for a sufficient length of time consistent
with the response characteristics of the radiation sensors.

One of the techniques which was found to satisfy these requirements
was the generation of the test gas by a blunt model immersed in the flow
region behind an incident shock wave produced by a sudden expansion of
driver gas in the electrically driven shock tube. The flow in the stagnation
region of such a model is characterized by the enthalpy and density cor-
responding to the incident shock velocity and the initial pressure of the
gas in the driven section of the tube. Consideration of one-dimensional
shock relations determines the direct correspondence to flight conditions.
In the present study a radiation sensor was located inside a model viewing
a well defined volume of uniform gas which extends from the model to the
bow shock.

The measurements in this configuration were based upon the develop-
ment of a system capable of sensing total radiant intensity integrated
over a complete wavelength spectrum including the far UV. A total radiation
cavity gage, used previously in radiation measurements through optical
windows was combined with a windowless, fast-acting shutter concept
resulting in a system capable to measure radiant energy down to the wave-
lengths corresponding to the photo-ionization edge of krypton (see Fig. 1.2)
used as a buffer gas in the space inside the model between the cavity gage
and the test gas.

1.3 Scope of Investigation

The unique feature of this work is the development and use of the fast response total radiation cavity gage system which permitted us to measure radiant intensity from a model shock layer through a non-absorbing optical path (except for the very short wavelength cut-off of the buffer gas). During the initial phases of the present study several problems developed in the readout of the gage signal which were traced to the severe conditions of the flow around the model. It was found that the partially ionized gas surrounding the model during the test had tendency to couple with the gage circuit causing distortion of the signal. This was further complicated by photo-emission of electrons within the gage which also affected the output signal. Considerable effort was therefore devoted to eliminate these effects which were successfully resolved in the course of the present investigation. Total intensity data were obtained at initial shock tube pressure P_1 = 0.33 torr and shock velocity range corresponding to flight velocities between 32,000 ft/sec and 45,000 ft/sec at relative density of the test gas ρ / ρ_o = 6 x 10^{-1}. The investigation includes measurements in the windowless configuration as well as with models equipped with quartz and lithium fluoride windows. The latter tests were intended to differentiate between the contribution from various regions of the wavelength spectrum. Proper interpretation of the experimental data required a considerable amount of analytical effort, mainly in the prediction of the total radiation as a function of density and temperature in the range of the experimental conditions.

These results were also used in deriving the implication of strong gas emission during Earth re-entry. In addition the effect of a large radiant energy flux emitted by the gas behind the bow shock on the properties of the gas in the shock layer has been analytically investigated, both for the shock tube and for a corresponding flight environment.

2. ANALYSIS

Because of the early interest in orbital and sub-orbital re-entry, considerable attention has been given in the past to the prediction of the radiance of air and similar gases at relatively long wavelengths - greater than about 1600 $\overset{o}{A}$ - and several experimental studies have been made to evaluate these results. At the temperatures above 8000°K and density levels of interest in superorbital entry, however, radiation at shorter wavelengths tends to become a significant part of the total energy emitted by the gas. This is partially due to the increased number density of atoms and charged particles which exhibit large absorption cross section for transitions from ground states. In addition the peak of the blackbody spectral distribution shifts towards shorter wavelengths allowing larger amounts of radiant energy emitted in this wavelength region to leave the volume of the radiating gas plasma. This was indicated in the theoretical results of Breene and his associates [1]; the implications of Breene's predictions in terms of radiative heat transfer at superorbital flight conditions were discussed by the present authors in Ref. 12.

In Breene's analysis, the major contributor to air radiance at $\lambda <$ 1600 $\overset{o}{A}$ is the electron-atomic ion recombination (free-bound) mechanism. Breene's simplified analytical model for this mechanism has been improved upon in the recent works of Sherman and Kulander [5] and Hahne [7].

Biberman and his associates have also conducted detailed studies of radiative heat transfer from air including mechanisms in the vacuum UV. A recent summary of their work is given in Ref. 3. Unfortunately, these results are presented quantitatively only in terms of integrated radiative flux so that the contributions of the different mechanisms to the total gas radiance can only be approximately deduced. Perhaps the most significant result of this work is the indication that atomic line radiation - mostly in the vacuum UV - will account for more than 50% of the total gas radiance over wide ranges of flow properties and radiating gas thickness of interest in the re-entry flight. This is shown in Fig. 2.1 where the relative contribution of lines as indicated by Vorobev et al (4) for a nitrogen plasma is shown.

2.1 Radiative Transfer

In considering the emission of electromagnetic energy from high temperature gases one must recognize that in most cases of interest including the present measurements the gas represents an extended source which has properties both of emission and absorption. That means that radiant energy emitted by one portion of the gas may be absorbed by another and shall never leave the control volume. When all emitted photons escape from the plasma we call it optically thin. Mathematical formulations of the radiative transfer under such conditions can be greatly simplified. Since the radiative properties of most plasmas are strong functions of frequency we find that in many cases the radiating gas may

be optically thin in certain spectral regions while strongly self-absorbed in others. It is therefore necessary to account for the spectral dependence of the emission and absorption when interpreting the observed intensity. On the assumption of LTE the effective absorption and emission coefficients at a given pressure and temperature can be related by recalling Kirchoff's law

$$\epsilon_\nu = \overline{\varkappa}_\nu \, B_\nu \qquad (2.1)$$

where

$$B_\nu = \frac{2h\nu^3}{c^2} \left(\exp\frac{h\nu}{kT} - 1 \right)^{-1} \qquad (2.2)$$

is the Flanck's function and the effective absorption coefficient,

$$\overline{\varkappa}_\nu = \left[1 - \exp\left(-\frac{h\nu}{kT}\right) \right] \sum_i (\varkappa_\nu)_i \qquad (2.3)$$

includes the correction for stimulated emission. We can therefore take the effective absorption coefficient, $\overline{\varkappa}$, as the primary property defining the radiative character of the plasma.

The quantity which is observed at a boundary point of the plasma is the intensity $I(\overline{r}, \vartheta, \nu)$ giving the power per unit area, per unit solid angle, in the direction specified by the angle θ and in the frequency interval ν to $\nu + d\nu$. By integrating the intensity with respect to the given variables we obtain total radiant energy flux, q_R, passing across a unit area of the enclosing surface. This quantity is required for the evaluation of radiative heating in the case of an entry vehicle. In the following

section we derive basic relations governing radiative transfer related particularly to the geometry of the present experiment and show the method applied in the interpretation of the experimental results.

For simplicity we can assume an isothermal and isotropic medium (this assumption is consistent with our experimental conditions). To calculate the emitted radiation we can consider an elementary volume dV within the gas which emits energy uniformly in all directions per unit time

$$4\pi \epsilon_\nu \, dV \, d\nu = 4\pi \, \bar{\varkappa}_\nu \, B_v \, dV \, d\nu \qquad (2.4)$$

Here $\bar{\varkappa}_\nu$ and hence ϵ_ν may depend on the coordinates of the given point. We are also assuming that the radiating gas is enclosed by perfectly transparent walls. Hence they do not reflect any radiation back into the gas. The fraction of the energy emitted by dV which would emerge through a unit area of the surface, S, enclosing the gas in the absence of self absorption is

$$\frac{\bar{n} \cdot (\bar{r}_1 - \bar{r})}{4\pi \, |\bar{r}_1 - \bar{r}|^3}$$

In this expression $\bar{n} \cdot (\bar{r}_1 - \bar{r})/|\bar{r}_1 - \bar{r}|$ is the projected unit area onto a plane normal to the ray emanating from the elementary volume, $\bar{n}$ is a unit vector normal to the surface, $\bar{r}$ is the position vector of the elementary volume dV and $\bar{r}_1$, is the position vector of the surface element dS.

PROJECTION

$\bar{k}$

$\bar{n}$

SURFACE
ELEMENT dS

$\bar{r}_1$

$\bar{r}_1 - \bar{r}$

$\bar{j}$

$\bar{r}$

RADIATING VOLUME
ELEMENT dV

$\bar{i}$

N103-663
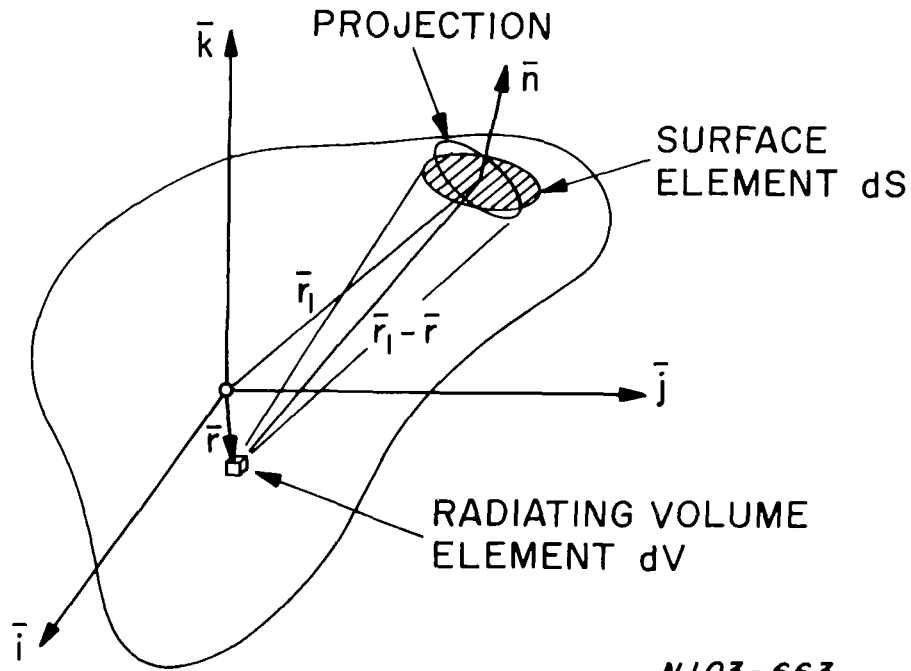
SKETCH A

In traversing the gas some of the energy is absorbed before it reaches

the boundary S of the gas.   The fraction of the transmitted energy through

the distance $|\bar{r}_1 - \bar{r}|$ is exp $(- \varkappa_\nu |\bar{r}_1 - \bar{r}|)$.   Thus the

monochromatic energy emitted by the elementary volume dV and actually

passing through dS is according to Lambert-Beer law

$$\frac{\varkappa_\nu B_\nu \bar{n} \cdot (\bar{r}_1 - \bar{r})}{|\bar{r}_1 - \bar{r}|^3} \exp (- \varkappa_\nu |\bar{r}_1 - \bar{r}|) \, dV \, d\nu$$

from which total energy emitted across unit area of the envelope is

-11-

$$q_{r} = \int_{o}^{\infty} \bar{\varkappa}_{\nu}\, B_{\nu} \int_{V} \frac{\bar{n} \cdot (\bar{r}_{1} - \bar{r})}{|\bar{r}_{1} - \bar{r}|^{3}} \exp(-\bar{\varkappa}_{\nu} |\bar{r}_{1} - \bar{r}|)\, dV\, d\nu \qquad (2.5)$$

It can be seen that besides depending on the radiative properties, the radiant energy is also strongly dependent on the geometry of the radiating gas. It is clear that in order to avoid complicated integral inversion procedures and to assure the greatest accuracy of the experimental results it is essential to restrict the plasma to the simplest possible geometrical configuration.

In the present study the use of the shock layer formed ahead of a blunt model in the flow behind an incident shock wave permits an approximation of the radiating gas by a semi-infinite parallel layer as shown below.
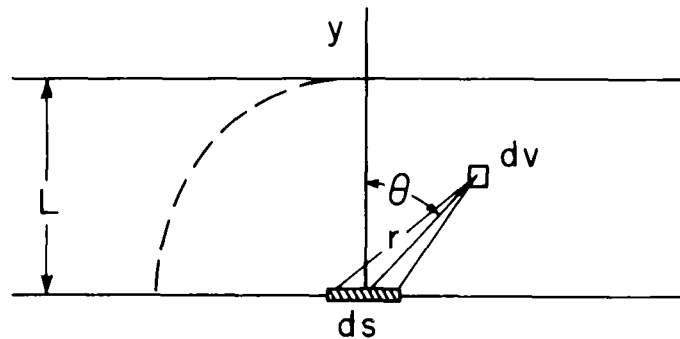
SKETCH B

The radiative energy passing through a unit area at the origin from all directions is obtained from 2.5 by taking $r_{1} = 0$ and substituting

for the elementary volume

$$dV = 2\pi r^2 \sin\theta \, d\theta \, dr \qquad (2.6)$$

together with

$$\frac{\overline{n} \cdot \overline{r}}{|\overline{r}|} = \cos\theta$$

To obtain the required quantity the integration must be carried out over the limits for r between 0 and ∞ and for θ between 0 and $\pi/2$. The integral can be divided into two parts

$$q_r = q_r^{(1)} + q_r^{(2)} \qquad (2.7)$$

where

$$q_r^{(1)} = \int_0^\infty \int_0^{\pi/2} \int_0^L \overline{\varkappa}_\nu B_\nu \, \sin 2\theta \exp(-\overline{\varkappa}_\nu r) \, dr \, d\theta \, d\nu \qquad (2.8)$$

and

$$q_r^{(2)} = \pi \int_0^\infty \int_L^\infty \int_{\cos^{-1}\frac{L}{r}}^{\pi/2} \overline{\varkappa}_\nu B_\nu \sin 2\theta \exp(-\overline{\varkappa}_\nu r) \, dr \, d\theta \, \nu \qquad (2.9)$$

which become upon integration

$$q_r^{(1)} = \pi \int_0^\infty B_\nu \left[1 - \exp(\overline{\varkappa}_\nu L) \right] d\nu \qquad (2.10)$$

and

$$q_r^{(2)} = \pi \int_0^\infty \overline{\varkappa}_\nu B_\nu L \int_1^\infty u^{-2} \exp(-\overline{\varkappa}_\nu L u) \, du \, d\nu \qquad (2.11)$$

with $u = r/L$.

We recognize that $q_r^{(1)}$ represents the contribution from the gas within the hemispherical volume with a radius L. The second integral, $q_r^{(2)}$, gives thus the radiant energy emitted by the remaining part of the semi-infinite layer. It is interesting to examine the limiting cases. In the case of an optically thin layer typified by $\bar{\varkappa}_\nu L << 1$ both integrands in $q_r^{(1)}$ and $q_r^{(2)}$, tend to $\bar{\varkappa}_\nu B_\nu L$ resulting in

$$q_r \rightarrow 2\pi L \int_0^\infty \bar{\varkappa}_\nu B_\nu \, d\nu \tag{2.12}$$

When the optical thickness $\bar{\varkappa}_\nu L > 1$ we have strong self absorption. The integrand in $q_r^{(2)}$ tends to zero and the energy passing through the unit area reduces itself to black-body radiation

$$q_r \rightarrow \pi \int_0^\infty B_\nu \, d\nu = \sigma T^4 \tag{2.13}$$

In any intermediate case

$$q_r^{(1)} \leq q_r \leq 2 \, q_r^{(1)} \tag{2.14}$$

The equation governing the radiative transfer in the direction normal to the planes bounding the radiating gas (Sketch B) is obtained from (2.5) by taking $\theta = 0$. It results in the expression for intensity

$$I = \int_0^\infty B_\nu \bar{\varkappa}_\nu \int_0^L \exp(-\bar{\varkappa}_\nu r) \, dr \, d\nu \tag{2.15}$$

-14-

Integrating with respect to y results in

$$I = \int_0^\infty B_\nu \left[1 - \exp(-\bar{\varkappa}_\nu L) \right] d\nu \qquad (2.16)$$

By comparing this expression with eq. (2.10) we see that the intensity in

the direction normal to the base is equal to $q_r^{(1)}/\pi$. By the nature

of the experimental configuration (collimated field of view), it is this

expression which is used in the interpretation of measured data.

2.2 Total Radiation of Air

The work of Biberman (3) appears to represent one of the more

complete treatise in which all presently known molecular and atomic

processes were included with a considerable attention given to their

spectral dependence. Hence no approximations frequently employed

such as grey gas or optically thin layer were introduced in the formu-

lation of the radiative transfer. The results therefore display the

typical self absorption characteristics at high relative densities and

large gas layer thicknesses. It is instructive therefore to analyze

further these results in order to make them more suitable for general

application.

The computations of Biberman have been presented in the form of

emissivity of a semi-infinite parallel and homogenous gas layers defined

by the expression

$$\bar{\epsilon} = \frac{q_r}{\sigma T^4} \qquad (2.17)$$

In arriving at the absorption coefficients of the elementary processes assumption was made of local thermodynamic equilibrium.

In attempting to correlate the given values of $\bar{\epsilon}$ as a function of pL, where p is the plasma pressure and L is the geometrical thickness of the gas layer, we found that in a certain range of pressures and temperatures the calculations displayed an anomalous behavior. This can be seen in Figs. 2.2 and 2.3 which shows $\bar{\epsilon}$ at T = 12000°K and 14000°K respectively. The tabulated values indicate that

$$\bar{\epsilon}_{p = 10 \text{ atm, } L = 1 \text{ cm}} = \bar{\epsilon}_{p = 1 \text{ atm, } L = 10 \text{ cm}}$$

which occurs neither at lower nor higher pressures. Such behavior has no obvious physical reason. We have therefore interpolated the data with the help of a further cross-plot to obtain the level indicated by the dashed line. Data for T = 17000°K and 20000°K shown in Figs. 2.4 and 2.5 were found to be normal.

The general feature shown in this correlation is that the pressure and gas layer thickness are not equivalent over most of the pressure range except at very high pressures where strong self-absorption mitigates the spectral characteristics of the various radiating systems contributing to the total spectrum. The effect of pressure change at a constant temperature is of course not only associated with changes of total particle density but also with changes of the chemical composition of the gas.

Since results of Biberman give q_r the quantity measured in the present study can be inferred by recalling that

$$\frac{q_r}{2\pi} \leq I \leq \frac{q_r}{\pi}$$

as derived in the preceding section. This establishes a range within which the intensity, I, will lie.

Allen (11) also performed theoretical calculations of the intensity normal to a semi-infinite slab using the technique which was employed in Ref. 6. These calculations include essentially the same radiating systems which were included in the prediction of Biberman although the treatment of individual systems may possibly be different. The results of Refs. 3 and 11 will be used for comparison with the present experimental data.

Several other theoretical predictions of high temperature air radiation are presently available but no attempt is made here to discuss the advantages of one set of calculations over the other.

2.3 Coupling Between Radiative Transfer and Flow

An important characteristic of the vacuum UV radiating mechanisms is their high absorption coefficient level which causes the predicted vacuum UV radiation to be strongly self-absorbed in a shock layer at flight conditions of interest while the same layer will be essentially transparent to radiation at longer wavelengths. This is illustrated in Fig. 2.6 for continuum radiation at $T = 14000^{\circ}K$ and $p = 1$ atm, using absorption

coefficients from Ref. 3. Similarly the relative contribution by ultraviolet lines is strongly influenced by self-absorption. Thus, at a given velocity and altitude a thin layer may be dominated by the vacuum UV contribution and a thick layer by the long wavelength radiation. The predicted effects of self-absorption on radiative heat transfer are shown in Figs. 2.7 and 2.8. In Fig. 2.7 we have presented the total equilibrium radiative heating predictions of Ref. 3 for a range of R_N values and over a range of flight velocities and altitudes. The predictions of Serbin (13) were used to determine the shock detachment distance and no correction was made to account for the curvature of the shock layer. The theoretical data have been normalized by $R_N^{0.6}$ and it is seen that this is a reasonably good correlation parameter for an important flight regime. For a shock layer transparent to all wavelengths, the correlation parameter would be simply R_N. Thus, the overall effect on total radiative heating of self-absorption is reasonably well approximated by assuming that the radiation is proportioned to $R_N^{0.6}$ (for this flight regime and the assumptions of the theoretical results, of course). Note that this result does not justify assumptions of the type that assign a wavelength averaged property to the gas (such as absorption coefficient or emissivity) and uses this property for further analysis; that is, the fact that the absorption coefficient is a strong function of wavelength must, in general, be factored into any detailed analysis of radiative transfer through, or out of, a heated gas region.

Figure 2.8 allows us to compare the predictions of different authors and assess the importance of absorption on radiative heat transfer for a hypothetical flight situation. The upper two values were calculated from the Breene absorption coefficients for the entire wavelength range of interest. The effect of absorption was included in the second; it reduces the vacuum UV heating appreciably but has a negligible effect on the long wavelength contribution. The Biberman predictions, taken from Fig. 2.7, include the self-absorption effect. It is somewhat more than twice the Breene-Sherman-Kulander value which does not include line contributions; therefore, considering the importance of line radiation in the Biberman results, we can conclude that, at least for this flight situation, there is an approximate agreement between the Biberman, et al and the Breene-Sherman-Kulander predictions for those mechanisms considered in the latter analysis.

In addition to self-absorption, we must consider the fact that the energy radiated from the shock layer will reduce the total energy level of the layer and thus cause the radiated energy to be lower than that calculated on an isoenergetic shock layer assumption. This can be referred to as the coupling of radiation and convection (14). Results of analytical studies of this effect have been presented by Goulard (14), Howe and Viegas (15), Hoshizaki and Wilson (16), Wilson and Hoshizaki (17) and the results of Refs. 15 and 17 have been compared in Ref. 16. These theories assumed that the gas was either transparent (14) (16) (17)

or a grey body (15) (they did not treat the self-absorption characteristics as a function of wavelength), so that their results must be considered to be only an approximation of the magnitude of coupling effects. Recently Hoshizaki and Wilson (18) published a theoretical approach to the radiating shock layer problem including the effects of coupling with wavelength dependent absorption and including the effects of viscosity.

The ratio of the uncoupled energy radiated from a heated gas region to the flow energy flux through that region is often used to indicate conditions at which important coupling effects can be expected. For a thin shock layer, this ratio can be defined as

$$\Gamma = \frac{2 q_{r_u}}{\dfrac{\rho_\infty U_f^3}{2}}$$

We have indicated lines of constant Γ on Fig. 2.7 for two spherical body nose radii. It is seen that for bodies in the interesting R_N range, the value of Γ can be of the order of 0.1 at velocities below the escape value. Since this Γ value represents a large decrease (25% or more) in radiative heating according to the theories mentioned above, we can be concerned that coupling effects might be significant in important flight situations.

Intuitively, it seems reasonable to expect that the reduction in radiative heat transfer due to coupling for a blunt body flow will primarily be a function of Γ , at least for the isothermal gas assumption. To

check this we have conducted a simple analysis for shock layer thickness

range of 1 to 10 cm. First, the Biberman q_{r_u} values were calculated

for a given flight condition; second, the radiated energy loss was assigned

uniformly across the shock layer (transparency assumption) resulting in

a lower average stagnation region enthalpy; third, a q_{r_c} value for the

new effective stagnation conditions was calculated; and fourth, the pro-

cedure was iterated until the convergence of q_{r_c} was achieved. Following

this approximate procedure, it is indeed found that the percentage radiative

heating reduction apparently is only a function of Γ; the result is given

in Fig. 2.9. Also shown in the figure are several results from Refs. 15

and 16 (as given in the latter). The good agreement between these results

and the present analysis fortifies the conclusion that Γ is the important

variable and suggests that the assumptions used in the three calculation

procedures are equivalent. However, Ref. 14 predicts considerably more

reduction in radiative heating as a function of Γ than shown in Fig. 2.9

(e. g., $q_{r_c}/q_{r_u} = 0.5$ at $\Gamma = 0.05$). Finally, we again emphasize that these

conclusions are not necessarily valid for a gas that has a strong wavelength

dependence of self-absorption. It is unfortunate that data published in

Ref. 18 do not allow us to calculate q_{r_c}/q_{r_u} and compare them with other

results in Fig. 2.9.

An interesting property of the coupling parameter can be seen through

analysis of a hypothetical entry vehicle trajectory. Fig. 2.10 shows the

velocity-altitude trajectory (simple ballistic) of a $R_N = 1$ ft. body that

enters the atmosphere at 40,000 ft/sec. We have also shown the uncoupled

heating predictions of Biberman and the coupling parameter based on these

predictions. From the shape of these curves, it can been seen that the

peak coupling parameter point precedes the peak uncoupled radiative

heating point by several seconds. This is seen in Fig. 2.11 where Γ

and q_{r_u} are plotted as functions of time. If we now make the assumption,

discussed above, that the percentage reduction in radiative heating at any

point on the trajectory is only a function of Γ , we conclude that the

coupling effect will not only reduce the radiative heating but also shift

the maximum heating point (and the centroid of the heating pulse area)

somewhat to later times than indicated by an uncoupled prediction. This

property is illustrated in Fig. 2.11 through plots of the coupled heating,

q_{r_c}, as determined from Fig. 2.9 and Ref. 14 again assuming that

q_{r_c}/q_{r_u} is only a function of Γ . The approximate coupling correction to

the Biberman prediction, based on Ref. 14 was also shown in Fig. 2.8.

From this brief discussion we conclude that radiative contributions

in the vacuum UV region of the spectra (nominally defined here as 500

to 1600 $\overset{o}{A}$), self-absorption of the shock layer gas, and coupling between

the radiated energy and flow energy are of potential importance in the

study of radiative heating to entry vehicles in superorbital flight regime.

In a sense, the existence of strong vacuum UV radiation promotes the

importance of self-absorption and coupling, since it is radiation at these

wavelengths that has large absorption coefficients, and since the coupling

parameter at a given velocity-altitude point is proportional to the total

energy radiated away.

3.   EXPERIMENTAL FACILITY AND INSTRUMENTATION

3.1   Facility Description

In the study of radiative properties of high temperature gases one is confronted with the problem of producing well defined samples of the gas at appropriate temperature and pressure levels for time durations compatible with the response characteristics of the radiation sensors. In the case of model measurements, this must be long enough to allow the formation of steady flow around the model. The simulation of conditions corresponding to hypervelocity entry has become possible with the development of the electrically driven shock tube (19) (20). The facility used in this study is shown in Fig. 3.1. It is essentially a conventional shock tube in which the driver remains isolated from the test gas present in the low pressure driven section by means of a mental diaphragm until the heating process of the light gas in the driver - an electrical discharge of capacitor stored energy - is completed. The design features and mode of operation have been discussed at length in Refs. 12 and 21. The driver tube in which the test section is located has a 6-in. i.d. and is 31.5 ft. long. Two capacitor banks, one rated at 304,000 joules and the other at 764,000 joules are available to supply the energy. The driver dimensions may be varied in size up to a 3 in. in diameter and 4-1/2 ft. in length by appropriate liner inserts. Fig. 3.2 is a photograph of the test section portion of the driven tube and shows some of the instrumentation used with the facility.

Fig. 3.3 illustrates the instrumentation techniques used to determine

the shock tube performance; also indicated are the techniques used to

measure total gas radiance both behind the incident shock wave and in

the stagnation region of a blunt model immersed in the flow produced by

the passage of the incident shock wave. The present measurements were made

using the flow ahead of blunt models only.

To determine the test flow properties and to assure validity of the

data during each run, several measurements are made. Signals from a

series of photomultipliers located at various stations along the shock tube

are used to measure the incident shock wave velocity as a function of

distance from the diaphragm. From this and the initial shock tube pressure,

the properties of the gas in any particular flow region are determined

using thermochemical equilibrium shock tube calculations. The techniques

used for assessing the quality of the test flow are dependent on observations

(from the sidewall of the shock tube) of the radiant emission from the gas

behind the incident shock wave and from the flow in the stagnation region

of the model. Since the emission is a strong function of temperature, the

temporal quality of the flow, in terms of its thermodynamic properties,

and its duration can be deduced from the steadiness of the emitted radiation,

and its spatial quality, from the image converter photographs. Instru-

mentation details and tube performance data are further discussed in

Refs. 12, 19, 21, 22 and 23.

In view of the discussions in the last section, it is interesting to

consider shock tube performance in terms of flight condition simulation.

This has been done in Fig. 3.4. Shown are sets of incident shock velocity-

initial tube pressure data taken with different size driver tubes (represented

by the nominal driver energy density values). Scales showing flight velocity

and approximate altitude simulation achieved in the blunt model stagnation

region are given on the figure.

The use of a larger capacitor bank (768 kj) allowed us to extend our

operational range of the facility to flight velocity simulation of approximately

60,000 ft/sec. The capabilities of this arrangement are shown in Fig. 3.5

where driver energy density is presented as a function of shock velocity.

Shown on the figure are experimental points obtained with either energy

bank and several shock tube initial pressure, p_1. The high velocity

points follow the general trend established at lower shock velocities for

the given initial pressure. On the right hand side of the figure we have

shown the operating range of our facility. The "A" energy bank has avail-

able 304 kj at 40 kv, while the "B" energy bank can supply 768 kj at the

same voltage. The energy density in the driver can be adjusted either by

reducing the voltage to which the capacitor bank is charged or by modifying

driver length. It can be seen from Fig. 3.5 that with a length of the driver

equal to 12 inches the "B" bank is capable of producing shock velocities

in excess of 44,000 ft/sec at a sufficiently high initial pressure necessary

to guarantee a positive duration of the test flow.

In Section 2.3 we discussed the occurrance of coupling between the

flow field and radiative energy transfer resulting in a non-adiabatic flow of the gas in the region of the stagnation point. It was shown that a parameter Γ , defined as the ratio of the radiative flux arrived at by the adiabatic consideration of the shock layer to the energy convected across the bow shock wave, gives useful indication of the magnitude of the coupling. In Fig. 3.6 we show the range of Γ which can be reproduced in the shock tube experiment using a 2-in. diameter blunt model.

To facilitate interpretation of the experimental data we are showing in Figs. 3.7, 3.8 and 3.9, the stagnation pressure, temperature and enthalpy taken from Ref. 24 and corresponding to the model configuration in a shock tube as functions of the incident shock velocity and the initial driven tube pressure. Conversion to flight velocity simulation is also given in Fig. 3.9. Multiplication of the shock velocity by a factor of 1.37 gives the flight velocity corresponding to the same stagnation enthalpy.

3.2   Total Radiation Cavity Gage

The measurement of total radiative heat flux from a high temperature gas volume across the surface enclosing it has always been a difficult problem. Its difficulty is further increased when the lifetime of the uniform radiation source is of the order of microseconds. Photoemissive devices such as photomultipliers and phototubes characterized by an extremely fast response are sensitive only to radiation over relatively narrow wavelength ranges. A suitable sensor in this respect

is a thin film resistance thermometer similar to the ones widely used for convective heat transfer in shock tubes and shock tunnels (25). Since such a gage depends on absorption of the radiant energy, a very serious drawback is the unknown reflectivity of its surface which is a function of the surface finish conditions, the wavelength of the incident radiation and the incident angle. Coating of the thin film thermometer, in most cases consisting of sputtered platinum, by low reflectivity materials such as carbon or gold, requires experimental verification of the degree of absorption at various wavelengths and incidence angles. It can also slow down the response of the gage beyond its usefulness for the shock tube application. For this reason we have selected a gage of the shape shown in Fig. 3.10 so that almost all radiant energy which enters the cavity can be absorbed by undergoing multiple reflections. Figure 3.11 shows the photograph of a complete gage. Details of analytical considerations leading to the given geometry and the mode of operation of the cavity gage have been given in Ref. 26. The platinum film is sputtered on the quartz substrate in a conventional way to approximately 1000-1200 $\overset{o}{A}$ thickness. Transmission of such a film was measured to be less than 2% in the wavelength range between 0.4 and 0.6 μ . At shorter wavelengths it becomes smaller. Calculations were made also of the delay in gage response due to the platinum film thickness using the approach given in Ref. 27. The results are shown in Fig. 3.12 from which we find that in our case the gage response is within 8% of the true value at 5 μ s for

a constant heating rate.

The thin film resistance thermometer, the sensor of the cavity gage, is operated at essentially a constant current in a circuit shown in Fig. 3.13. Each lead is connected through a large resistor to a dry cell battery pack while the signal is fed into a differential amplifier to reject any common mode noise pick-up.

As we show in Ref. 26 the heat flux to the film can be deduced from the temperature history of its surface and is given by

$$q(t) = \pi k\rho c \left\{ \frac{T(t)}{2\sqrt{t}} + \frac{1}{2\pi\sqrt{t}} \int_0^t \frac{\sqrt{\lambda}\, T(t) - \sqrt{t}\, T(\lambda)}{(t - \lambda)^{3/2}}\, d\lambda \right\} \tag{3.1}$$

The temperature change of the platinum film during the experiment, $T(t)$, is obtained by measuring the resistance of the film, $R(t)$, as a function of time. To convert it to temperature we require the value of the thermal coefficient of resistivity, α. This is determined by static calibration in a controlled environment over a range of temperatures encountered during the radiation measurements.

Thus the temperature change, $T(t)$ is

$$T(t) = \frac{\Delta R(t)}{\alpha R_o}$$

or $\hspace{10cm}$ (3.2)

$$T(t) = \frac{\Delta V}{\alpha i R_o}$$

-29-

A computer code has been written which performs the necessary integration in Eq. (3.1) for a given input of gage voltage history and particular characteristics of the given gage such as α and R_0. A typical oscilloscope trace of the cavity gage signal is shown in Fig. 3.14. The characteristic parabolic shape is associated with a constant heat transfer rate to a thin film thermometer gage.

In Ref. 26 we have also derived the pertinent formula relating the observed output signal of the gage and the radiative energy flux incident on the entrance opening.
This is given by

$$O(t) = A_g \, q(t) \tag{3.3}$$

where A_g is the effective area of the sensing element (platinum thin film). The corresponding history of the radiative flux is determined by the reduction of gage output signal as shown in Fig. 3.15.

3.3   Cavity Gage System with Windows

The total radiation cavity gage has been used in a shock tube in two experimental configurations with solid windows separating the gage from the radiating gas sample. In one, measurements are made of radiation emitted by the gas processed by the incident shock wave (28). The gage is located behind a set of collimating slits veiwing only a narrow layer of gas normal to the axis of the shock tube. Splitter plates have been used to allow the variation of the optical depths and to eliminate the uncertainty

of effects caused by either absorption or emission in the boundary layer. In all recent investigations, quartz windows were used to separate the radiating test gas from the gage. Because of the limit of the temperature and density which can be obtained with the available input energy into the driver, the gas radiance at temperatures above $12,000^{\circ}K$ has been measured using the stagnation point shock layer gas as the gas sample. The arrangement of the total radiation cavity gage inside a cylindrical flat face model is shown in Figure 3.16. A circular window, 1 mm thick, was mounted in front of a rectangular slit, 0.1 in. by 0.5 in., flush with the face of the model. The gage itself is located away from the window with its entrance slit parallel to the window aperture, viewing only the gas in the shock layer close to the axis of the model. A similar arrangement of the gage is used in a hemispherical model.

During initial operation of the gage, evidence of photoemission from the platinum film was observed (22). During tests in which the gage was evacuated to a pressure of approximately 3 microns, the photoelectric effect was strong enough to produce partial short-circuiting of the gage. A few runs were made with a glass window under the same flow conditions with no evidence of the photoelectric effect, indicating that photons with energy corresponding to a wavelength smaller than 3500 $\overset{o}{A}$ are required to cause the photoemission. To eliminate this effect, the gage was filled with pure nitrogen at 1 atm pressure. The presence of the nitrogen gas reduced the mean free path of the electrons, causing a space charge to

develop close to the surface of the gage within a fraction of a microsecond from the arrival of the incident shock. This space charge apparently inhibited any further electron emission. Nitrogen gas was chosen because of its large cross-section for collision with electrons.

3.4   Development of Windowless Gage System

As was stated before the main purpose of the present investigations was the measurement of total thermal emission from air at temperatures above $12,000^O$K. Referring to Fig. 1.2 we note that in such a case a large part of the radiant energy emitted by the plasma will be at wavelengths within the vacuum UV region of the spectrum.

Materials normally used for windows in shock tubes, including quartz, have distinct short wavelength transmission cut-offs. These cut-off values, as shown in Fig. 1.2, occur at wavelengths longer than much of the radiation of interest in high temperature gas radiance studies. Therefore, a measurement system with a windowless capability is suggested.

The use of N_2 is satisfactory behind sapphire and quartz windows; however, for studies of vacuum UV radiation, N_2 is not suitable because of its photoabsorption characteristics (see Fig. 1.2). In this case, the choice is limited to rare gases, with helium and argon displaying the most desirable optical properties. (The cut-off for helium, not shown in Fig. 1.2 occurs at about $190,000$ cm^{-1}). The ability of the buffer gas to suppress the photoelectric effect was evaluated using a model with

-32-

a LiF window. As a first choice, argon at 2 atm pressure was used. A cavity gage signal obtained from this run is shown in Fig. 3.17. The presence of a photoelectric effect which causes the signal to become negative for the duration of the test flow is evident. The inability of argon to adequately reduce the electron emission can be explained by referring to Fig. 3.18 where electron collision cross-sections for several gases are plotted as a function of electron velocity (29). Although argon and krypton display cross-sections for electrons greater than nitrogen at electron energies above 4 ev, both are practically transparent to electrons with energies in the vicinity of 1 ev. This transparency, known as the Ramsauer-Townsend effect, is typical of the heavier rare gases. A gas mixture with equal proportions of Kr, having large cross-sections for energetic electrons, and He with a reasonable effectiveness for scattering slow electrons, was tried next in the model. A typical trace of the cavity gage response with the LiF window model is shown in Fig. 3.19. It can be seen that the strong photoelectric effect is absent and the signal trace is typical of a thin film thermometer response to an approximately steady heating pulse.

As previously mentioned, a windowless gage-model system is required for sensing vacuum UV radiation. Since a gas mixture within the model is necessary to counteract the photoelectric effect, the problem arises of how to contain this gas inside the model prior to the arrival of the incident shock wave and to prevent it from mixing appreciably with

the test gas. The results obtained earlier indicated that the gas density

inside the model must be considerably higher than the shock tube initial

pressure for an effective restriction of movement of the photoelectrons.

A windowless model as shown in Fig. 3.20 was therefore developed in

which a stretched latex membrane separates the model gas from the shock

tube. A pulse of current is passed through a 0.002 in. wire located along

the rectangular entrance slit and in contact with the latex membrane as

shown in Fig. 3.21. No combustion of the membrane nor melting of the

wire takes place, but the rapid heating weakens the latex to a point where

it tears under its own internal stress. The process of uncovering the

entrance slit of the model takes approximately 15 μs. Depending on the

gage gas pressure, a delay of about 140 μs between the current pulse and

full opening of the slit was observed. This delay was found to be repeat-

able within 10 μs. By using a delayed trigger signal from an upstream

station, the full opening process can be scheduled to be completed approxi-

mately 10 μs prior to the arrival of the incident shock wave at the model

station. Consideration of the inflow process in the case when the internal

pressure is much lower than the stagnation pressure indicated that it

would be difficult to account properly for the absorption characteristics

of the inflowing gas (unsteady and non-equilibrium expansion process in

the optical path). If the internal pressure is set equal to the stagnation

pressure this effect will ideally be eliminated; therefore, we have followed

the latter approach in our windowless system.

At the instant when the latex membrane breaks, the buffer gas issues through the entrance slit into the stationary gas in the shock tube. Since the breaking of the membrane occurs approximately 10 μs before the incident shock arrives at the model, only a small amount of the buffer gas escapes and its penetration is limited to a few centimeters upstream of the model. This gas is swept downstream during the first 1-2 μs after the incident shock arrives at the model (which is usually less than the time needed to form the quasi-steady blunt body flow). Additional advantage of being able to time the membrane opening to within about 10 μs of the shock arrival is that the expansion wave inside the model does not reach the gage and cause a convective perturbation within the flow test time. Assuming that the interface between the test gas and the gage gas is stationary, the diffusion of the gases across it was estimated to be negligible during the time corresponding to a typical test gas flow (20-30 μs).

A similar model with a 1-in. nose radius, shown in Fig. 3.22, was also built and used in the present study for two reasons. Firstly, it was intended to establish experimentally the dependence of the measured intensity, I, on the gas layer thickness (shock layer thickness for the hemispherical model is approximately 1/3 that of the cylindrical model) and secondly, at shock velocities above 33,000 ft/sec the formation of the blunt model flow for the cylinder consumes too much test time leaving marginally little time for the response of the gage to the uniform flow.

4. EXPERIMENTAL PROCEDURES

In this section we shall describe the techniques employed in preparation of the experimental conditions leading to the acquisition of data. This includes the preparation of the test gas in the shock tube as well as the steps involved in setting up the model and the radiation gage.

4.1 Test Flow Determination

During the present experimental study stringent precautions were taken to ensure that the contamination of the test gas was at a minimum. A thorough cleaning of the tube with methyl alcohol and dry, clean rags preceded 2-3 hrs. pumping period prior to each test. The tube was normally evacuated down to approximately 8μ and kept at this pressure to promote outgassing of the walls. A leak check taken at that pressure indicated normally a rate of $0-0.8\mu$ per minute. The tube was then filled with the test gas to the pressure level required for the experiment. Bottled dry air (-75°F dew point) produced by the Matheson Co. was used in the driven tube. In order to further reduce the contaminants due to outgassing of the shock tube walls a through-flow system was provided. This allowed a continuous scavenging of the tube at test pressure level for approximately 30 minutes prior to the actual run. The test gas was introduced through a cold trap of dry ice and acetone at the diaphragm end of the tube while a mechanical vacuum pump at the model end produced the through flow. With the cold trap temperature of -78°C the moisture present in the test gas was reduced down to 0.005%.

The through-flow was shut off 2-3 min. prior to the run and the pressure adjusted to the required level and read by means of a McCleod gage located at the center of the tube length.

The thermodynamic state of the test flow is determined from the shock velocity and the initial driven tube pressure. The shock speed is obtained by observing the luminous profile of the shock wave with collimated photomultipliers as it passes seven stations ahead of the test section at which the model is located. The time-of-arrival signals from each photo-sensor are differentiated and displayed on a raster trace. The arrival of the shock front at each station can be read with an accuracy of about ± 0.5 μs which for example, at 30,000 ft/sec gives shock speed with an accuracy of better than 1%. In addition ionization gages located at two stations were also used as a check of shock speed obtained from the passage of the luminous shock front. Typical shock speed data obtained from the raster display is shown in Fig. 4.1. Normally a good agreement between these two methods was observed. The change of shock velocity always gives an indication, in most cases appearing as attenuation, of a possible variation of flow properties.

The second important aspect of the flow is the available test time as determined by the length of the shock processed gas between the incident shock wave and the passage of the interface region separating the gas initially in the driven tube and the driver gas. It was found that the actual test time is much shorter than the prediction calculated on the

basis of viscous flow but neglecting turbulent mixing caused by the finite

opening time of the diaphragm. Also, it was found that the available test

time can differ from run to run as shown in Figure 4.2 although the test

conditions are kept the same. Measurements are normally taken during

each experimental run to determine the actual test time. It was shown in

Ref. 30 that such measurements should be based on at least two independent

methods. In the present study we used two techniques.

In the first one the emitted light from the shock heated gas behind

the incident shock wave is observed (30). The arrival of the shock front

is associated with a sudden appearance of strong radiation overshoot which

decays to an equilibrium level within a short time, as the gas relaxes

to the thermochemical equilibrium, and its temperature drops. The uni-

form level of the emitted energy corresponding to the test gas flow follows

until the contact zone arrives at which instant the test time ends. The

emission from the gas is a very strong function of its temperature.

Hence, the steadiness of the test gas emission is a good indication of its

quality.

Using a two-channel photometer the quality and the length of the

test time and the length of time necessary to establish steady flow around

the model is determined by monitoring the emission from the shock layer

ahead of the stagnation point of the model. This method is necessary

whenever model experiments are performed (30). Representative oscil-

loscope traces of the signals from the red channel photometer (0.5 - 1.0μ)

are shown in Figs. 4.3 and 4.4. The steadiness of shock layer intensity determines the quality of stagnation region flow. In most cases the blue signal shows an increase in intensity upon the arrival of the mixed gas in the contact zone while the red channel indicates a drop in radiation at its response wavelengths.

An image converter camera was also used, mainly to assess the quality of the flow by showing the shape of the incident shock wave and the symmetry of the model flow and to establish the volume of the radiating gas sample that contributes to the radiant energy sensed by the cavity gage. This is illustrated in Figs. 4.3 and 4.4 where photographs obtained from the windowless model with the camera set for a 0.050μ s exposure are shown. Each photograph contains three frames taken 5μ s apart. The lower traces in these figures show the camera monitor and photomultiplier signals. The photomultiplier looks through a window in the sidewall of the shock tube and is focused just ahead of the model stagnation point. In Fig. 4.4 the first image converter camera frame was obtained during the flow formation as indicated by the camera monitor. The next two frames were taken during the steady flow corresponding to an approximately uniform shock layer radiance and constant stand-off distance. These photographs also indicate that a uniform flow was achieved within the expected time (with the end of test gas flow clearly visible), and that the shape of the bow shock wave was not perturbed by the presence of the windowless slit at the stagnation point of the model.

4.2   Total Radiation Measurements

All total radiation measurements were made using the cavity gage described in section 3.2. The arrangement of the gage in the models was shown in Figs. 3.16 and 3.20. It was found necessary to shield the gage and the associated leads which are located in the sting in order to eliminate stray electrical pick-up during plasma flow. All quartz and lithium fluoride windows, used in the model, were 1-mm thick and were replaced for each run. They were also thoroughly cleaned with appropriate solvents after assembly of the model. Sample checks of the fused silica windows showed extremely good transmission (80%) down to 1700 $\overset{o}{A}$. Manufacturers specifications of lithium fluoride windows used in the present study indicated short wavelength cut-off at approximately 1100 $\overset{o}{A}$.

The windowless model was frequently calibrated to determine the opening delay of the latex membrane which is the time between the pulse of the current in the wire and the uncovering of the entrance aperture.

The output of the cavity gage was displayed on the oscilloscopes and photographed. Next the traces were enlarged and the time history of the gage resistance read. Representative oscilloscope traces obtained with the gage behind lithium fluoride and quartz windows are shown in Fig. 4.5. In both cases the model was filled with 50% Kr-50% He gas mixture at p = 4 atm.

In the case of the windowless model the pressure inside the model was set to the level of the stagnation pressure. A 66% Kr-34% He gas

mixture was used as the buffer gas inside the model. Oscilloscope traces of the gage signal from the windowless model are shown in Fig. 4.6.

The interpretation of the measurements depends on relating the observed energy rate, Q, entering the cavity gage with the dimensions of the radiating gas volume.

To formulate the required relations we can refer to the schematic representation of the gage and its position with respect to the radiating gas which in our case is the shock layer.
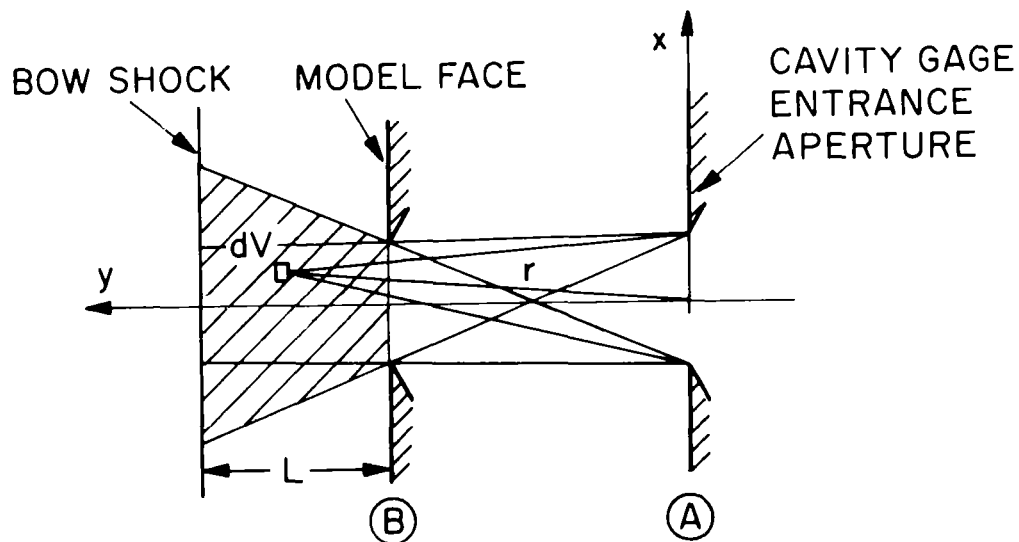
N103-662

SKETCH C

The gage entrance aperture is located in plane A while the field of view limiting aperture (model entrance slit) is in plane B.

-41-

Let us consider an elementary volume dV located at r=r (x, y, z)

distance from plane A. The monochromatic energy emitted by this volume

in all directions is

$$4\pi \; \bar{\varkappa}_\nu \; B_\nu \qquad\qquad (4.1)$$

of which a fraction $\Omega/4\pi$ will be intercepted in the absence of absorption

by the gage entrance aperture in plane A. Here $\Omega = \Omega$ (r) is the solid

angle extended by the gage aperture. Because of self absorption, however,

energy reaching the gage will be reduced to

$$dQ\,(\nu) = \bar{\varkappa}_\nu \, B_\nu \, \Omega(r) \, \exp\left[-\bar{\varkappa}_\nu \, (r-r_1) \right] dV \qquad\qquad (4.2)$$

This expression must be integrated over the whole radiating volume defined

by the field of view of the gage.

Thus

$$Q\,(\nu) = \bar{\varkappa}_\nu \, B_\nu \int_V \Omega(r) \, \exp\left[-\bar{\varkappa}_\nu \, (r-r_1) \right] dV \qquad\qquad (4.3)$$

For a collimated beam as is the case in the present configuration of the

gage we can assume r = y.

At each y position we can also define an average solid angle by

$$\bar{\Omega}\,(y) = \frac{\iint \Omega dx\, dy}{\iint dx\, dy} \qquad\qquad (4.4)$$

We have calculated the product of the average solid angle $\bar{\Omega}$ (y) and

the area, A_{xz} for the geometry used in the present experiments and found

that it is almost constant along the y axis and can be replaced by its

average value $\overline{\Omega A_{xz}}$. Hence Eq. (4.3) can be simplified to give

$$Q (\nu) = \bar{\varkappa}_\nu B_\nu \overline{\Omega A}_{xz} \int_{y_1}^{y_2} \exp\left[- \bar{\varkappa}_\nu (y-y_1) \right] dy \qquad (4.5)$$

from which

$$Q = \overline{\Omega A}_{xz} \int_{0}^{\infty} B_\nu \left\{ 1 - \exp\left[-\bar{\varkappa}_\nu L \right] \right\} d\nu \qquad (4.6)$$

with $y_2 - y_1 = L$. In Eq. (4.6) we recognize the integral to be equal to

radiant intensity, I_ν as was given in Eq. (2.28).

Therefore

$$I = \frac{Q}{\overline{\Omega A}_{xz}} \qquad (4.7)$$

Thus the intensity, I, can be obtained from the given Q, which follows

from the reduced gage signal and the gage geometry as outlined in section 3.2.

5.   DISCUSSION OF RESULTS

Data obtained from the shock tube blunt model test flow using the window and windowless cavity gage measurement techniques described in the last section are shown in Figs. 5.1 and 5.2. In Fig. 5.1 we have compared data obtained with quartz and LiF windows. The theoretical predictions of Breene ($\lambda > 0.16\mu$), which include free-free, free-bound and molecular band radiation, and results of Allen ($\lambda > 0.20\mu$) which also include bound-bound radiation, are shown.

Compared in Fig. 5.2 are experimental results obtained with quartz windows and with the windowless configuration (with He-Kr mixture as the buffer gas). Models used, as indicated by different symbols, were the 1.5 in.-diameter flat face model and the $R_N = 1$-in. hemispherical model. Theoretical results of Allen ($\lambda > 0.2\mu$ and all λ) and the results of interpretation of Biberman flux calculations for the shock tube conditions assuming a 1 cm stand-off distance are also shown. The latter one is represented by the cross-hatched band for reasons explained in Section 2.2. The data in Figs. 5.1 and 5.2 have been referenced to a 1 cm thick shock layer value from the shock stand-off distance measurements of 0.28 cm for the hemispherical model and 0.76 cm for the flat faced model to allow the results to be more easily compared. A theoretical correction of -9% due to self-absorption - is required by the windowless data to account for this adjustment. The indicated corrections to the window data are negligible because of low self-absorption at $\lambda > 0.2\mu$. A theoretical

correction of +10% in the windowless data to account for the short wavelength

radiation cut-off by Kr in the model nullifies essentially the correction for

self-absorption. Finally, a conservative estimate of self-absorption in the

stagnation region boundary layer was made at the velocity level of the

windowless tests and at a potentially severe absorption density level. An

apparent reduction in intensity of 8% was indicated for these conditions;

however, no correction for this effect has been made in the data.

First, in Fig. 5.2 it is seen that the windowless data are considerably

higher than those from the window models. The data show a large contri-

bution to the radiant intensity between the short wavelength cut-offs of

quartz and of Kr. Second, the quartz data are in a good agreement with

Allen predictions for $\lambda > 0.2\mu$. Although the quartz windows had a short

wavelength cut-off (calibration of several samples of those used in our tests

showed 80% transmission at 0.17μ) below the range of the theoretical

calculations, the contribution to intensity between 0.17μ and 0.2μ is

not considered to be significant. Breene's predictions which extend down

to $\lambda = 0.16\mu$ but do not include line radiation lie on the low side of the

experimental data suggesting that the line radiation in the visible and

infrared is 20% to the total intensity in this spectral range. This is

further confirmed by Nerem (31) who has compared the experimental

equilibrium intensity results for air of several investigators (32) (33) (34)

taken with solid windows with cut-off levels to as low as 0.17μ . He has

found a reasonably good agreement between these results including his data

and the long wavelength predictions of Breene. Third, the windowless

data lie in the range of the Biberman, et al predictions. Fourth, the

agreement between the quartz data for the different shock stand-off dis-

tance indicates that there is a negligible self-absorption effect at long

wavelengths (as expected). More importantly, since the normalized data

(to 1 cm gas layer thickness) for the small standoff distance should be

larger than those for the larger value if strong coupling effects were

present, these results imply that the effect of coupling is small for the

present test conditions (Γ is of the order of 0.1 for the flat faced body).

Of course, an effect of the order predicted in Fig. 2.9 could be hidden

within the scatter of the data in Fig. 5.2. Therefore, conclusions on the

importance of coupling in a radiating flow based on the present data must

be considered to be preliminary.

In Fig. 5.1, the quartz and lithium fluoride data comparison sug-

gests a higher intensity level in the latter case. However, we have

found LiF to be a difficult material to work with; the quality and, possibly,

the cut-off wavelength can vary from sample to sample. Examination of

the windows after test runs revealed that they were crazed. This problem

is of particular importance, since we have not determined if the crazing

occurs during the test time. Therefore, we believe that a definite con-

clusion cannot now be drawn from our data concerning the magnitude of

the contribution to the intensity (mostly UV lines) in the region between

the (potentially available) 0.11μ short wavelength cut-off usually quoted

for LiF and that for quartz. Present results contradict conclusion drawn

by Nerem (31) who, on the basis of several data obtained with LiF windows,

inferred that there is no substantial contribution to the total radiation

due to emission in the wavelength region of 0.12 to 0.17μ .

6.   SUMMARY OF RESULTS AND CONCLUSIONS

Results have been presented from a study of high temperature air

radiance over range of equilibrium gas properties of interest to super-

orbital re-entry vehicles; the following points are of interest: 1) radiation

in the vacuum UV region of the spectrum (defined here to be $\lambda < 1600 \overset{o}{A}$)

can be expected to be important; 2) because of the large cross section of

the radiative mechanisms in the vacuum UV, self-absorption in a radiating

gas layer must be included in the analysis of energy fluxes through such

a layer with a proper regard for the wavelength dependence of the absorption

coefficient; 3) coupling between the radiative and convective energy fluxes

may significantly reduce the total radiative heat transfer in comparison

to that calculated for an isoenergetic layer; however, the prediction of

such an effect is complicated by the wavelength dependent self-absorption

property of the gas; 4) analysis of total radiation predictions of Biberman

et al indicate a discrepancy which was corrected by correlating the given

data according to the product of pressure and gas layer thickness, pL;

5) a body scale parameter, $R_N^{0.6}$, has been found to approximately

correlate the uncoupled radiative flux of Biberman; the difference between

this dependence and that for a simple transparent shock layer gas, R_N,

indicates the integrated influence of self-absorption in the shock layer;

7) the predictions of Biberman result in relatively high values of the

coupling parameter ($\Gamma = 0.1$) for body dimensions of interest at velocities

of the order at the Earth escape value; and 8) for a simple type of entry

vehicle, Γ will maximize before the peak uncoupled heating point with the probable result not only in a reduction of radiative heating but also in a shift of the maximum radiative heating point to later times in the trajectory.

A shock tube experimental study has been conducted to investigate several of the total radiative properties of air. It has been shown that an electrically driven "conventional" shock tube is capable of producing useful model stagnation region test flows to the 60,000 ft/sec flight velocity simulation level. At such conditions, the Γ values for models of practical size are far in excess of 0.1, and therefore, important combined effects of self-absorption and coupling might be expected. A fast response total radiance measurement technique that employs a thin film cavity sensing element has been developed and used in the study. The cavity gage has been combined with blunt models that permit the sensing of energy radiated from the shock layer with and without solid windows in the optical path. In its windowless configuration, the measurement system as presently developed has a short λ cut-off of approximately 880 $\overset{o}{A}$. According to the available predictions, this permits the measurement of almost all radiation energy at the conditions of interest.

Experimental intensity data, obtained in the range of a simulated flight velocity between 38,000 and 49,000 ft/sec, show that there is a significant contribution to intensity in the vacuum UV portion of the spectrum. The windowless data tend to agree with the available total

-49-

radiance predictions that include spectral line contributions. Long wave-length data obtained with quartz windows are in fairly good agreement with the predictions of Allen for the corresponding wavelength regime. Also, there is an indication of a contribution to intensity in the wavelength region between the quartz and LiF cut-off values. A preliminary assessment of the coupling effect for the range of conditions studied suggests that it is hidden within the scatter of the present data.

The effects of the boundary layer have not been included in the present study except for the estimation of its importance in the absorption of energy radiated from the shock layer for a specific test condition. The boundary layer is of concern in flight situations not only because of this effect, but also because absorbed radiation will influence the boundary layer properties and, therefore, modify the convective heat transfer. This could be of particular importance for an ablating body where relatively complex molecules may exist near the surface of the body. A semi-empirical treatment of this problem, applied to the determination of the performance of ablation materials subjected to combined radiative and convective heating in superorbital flight, is given in Ref. 35.

References

1. Breene, Jr. R. G. and Nardone, M. C. , "Radiant Emission from High Temperature Equilibrium Air", J. Quant. Spectr. Radiative Transfer, 2, 272-292, (1962).

2. Breene, Jr. R. G. and Nardone, M. C. , "Radiant Emission in the Atmospheres of the Terrestrial Planets", Symp. on Dynamics of Manned Lifting Planetary Entry, (John Wiley & Sons, 1963). Also, private communication.

3. Biberman, L. M. , Vorobev, V. S. , Norman, G. E. and Iakubov, I. T. , "Radiation Heating in Hypersonic Flows", Kosmich Issled, 2, 441-454 (1964).

4. Vorobev, V. S. and Norman, G. E. , "Energy Radiated in Spectral Lines by an Equilibrium Plasma", Optical Spectr. 17, 180 (1964).

5. Sherman, M. F. and Kulander, J. L. , "Free-Bound Radiation from Nitrogen, Oxygen, and Air", General Electric Co. , MSD Report TIS R65SD15 (May 1965).

6. Allen, R. A. , "Air Radiation Graphs: Spectrally Integrated Fluxes Including Line Contributions and Self-Absorption", Avco-Everett Research Lab. Report 231 (September 1965).

7. Hahne, G. E. , "The Vacuum Ultraviolet Radiation from N' and O^+ Electron Recombination in High-Temperature Air", NASA TN D-2794, (June 1965).

8. Armstrong, B. H. , Johnston, R. R. and Kelley, P. S. , "Opacity of High Temperature Air", Lockheed MSC, Rept. 8-04-64-2 (November 1964).

9. Wilson, K. H. and Greif, R. , "Radiation Transport in Atomic Plasmas", Lockheed MSC, Rept. LMSC 6-77-67-31 (November 1967).

10. Page, W. A. , Compton, D. L. and Borucki, W. J. , "Radiative Transport in Inviscid Nonadiabatic Stagnation-Region Shock Layer", AIAA Paper 68-784 (June 1968).

11. Allen, R. A. , "Total Air Radiation Calculations and Comparison with Recent Measurements", AIAA J. , 5, 589-590 (1967) and private communication (1967).

12. Gruszczynski, J. S. and Warren, W. R. , "Experimental Heat Transfer Studies of Hypervelocity Flight in Planetary Atmospheres", AIAA J. , 2, 1542-1550 (1964).

13. Serbin, H., "Supersonic Flow Around Blunt Bodies", J. Aerospace Sci. 25, 58-59 (1958).

14. Goulard, R., "The Coupling of Radiation and Convection in Detached Shock Layers", J. Quant. Spectr. Radiative Transfer, 1, 249-257 (1961).

15. Howe, J.T. and Viegas, J.R., "Solutions of the Ionized Radiating Shock Layer, Including Reabsorption and Foreign Species Effects, and Stagnation Region Heat Transfer", NASA TR R-159 (1963).

16. Wilson, K.H. and Hoshizaki, H., "Inviscid, Nonadiabatic Flow About Blunt Bodies", AIAA J. 3, 67-74 (1965).

17. Hoshizaki, H. and Wilson, K.H., "The Viscous, Radiating Shock Layer About a Blunt Body", AIAA J. 3, 1614-1622 (1965).

18. Hoshizaki, H. and Wilson, K.H., "Convective and Radiative Heat Transfer During Superorbital Entry", AIAA Paper 66-106 (January 1966).

19. Warren, W.R., Rogers, D.A. and Harris, C.J., "The Development of an Electrically Heated Shock Driven Test Facility", General Electric Co.,Report TIS R62SD37, (April 1962). Also, Proceedings of the 2nd Symposium on Hypervelocity Techniques (University of Denver, Colo., March 1962).

20. Camm, J., "Escape Velocity Shock Tube with Arc Heated Driver", Proceedings of the 2nd Symposium on Hypervelocity Techniques (University of Denver, Colo., March 1962).

21. Gruszczynski, J.S., Warren, W.R. and Diaconis, N.S., "Laboratory Simulation of Hypervelocity Heat Transfer Problem During Planetary Entry", General Electric Co., Report TIS R64SD73 (November 1964).

22. Gruszczynski, J.S., Warren, W.R. and Rogers, D.A., "Shock Tube Techniques for Studies of High Temperature Gas Radiance", Proceedings of the 5th Shock Tube Symposium (U.S. Naval Ord. Lab., Silver Spring, Md., April 1965). Also General Electric Co., Report TIS R65SD33 (August 1965).

23. Gruszczynski, J.S. and Rogers, D.A., "Shock Tube Instrumentation Techniques for Study of Hypervelocity Entry Problems", General Electric Co., Report TIS R64SD67 (Sept. 1964).

24. Laird, J. D. and Heron, K., "Shock Tube Gas Dynamic Charts",
    Part I: Equilibrium Argon-Free Air From 3000 to 10,000°K, AVCO
    RAD Technical Memorandum RAD-TM-64-12 (April 1964).

25. Vidal, R. J., "Transient Surface Temperature Measurements",
    Cornell Aeronautical Lab., Report. No. 114 (March 1962).

26. Gruszczynski, J.S., Harris, C.J., Rogers, D.A. and Warren, W.R.,
    "Fast Response Total Radiation Gage for Measurement of Radiant
    Emission from High Temperature Gas", General Electric Co., Report
    TIS R63SD11 (January 1963). Also IEEE Conf. Paper No. 63-438
    (January 1963).

27. Vidal, R. J., "Model Instrumentation Techniques for Heat Transfer
    and Force Measurements in a Hypersonic Shock Tunnel", Cornell
    Aeronautical Lab., Report No. AD-917-A-1 (February 1956).

28. "Hypervelocity Heat Transfer Studies in Simulated Planetary Atmo-
    spheres", General Electric Co. Final Report, Jet Propulsion Lab.
    Contract 950297 (June 1967).

29. Massey, H.S. and Burhop, E.H.S., "Electronic and Ionic Impact
    Phenomena", (Oxford at the Clarendon Press, 1952).

30. Gruszczynski, J.S. and Rogers, D.A., "Shock Tube Instrumentation
    Techniques for Study of Hypervelocity Entry Problems", IEEE/PTGAS,
    Proceedings of the 1st International Congress on Instrumentation in
    Aerospace Simulation Facilities, Paris, France (1964). Also General
    Electric Co., Report TIS R64SD67 (September 1964).

31. Nerem, R.M., "Radiating Flows Around Re-entry Bodies", presented
    at the XVIth International Astronautical Congress, Athens, Greece,
    Reprint No. 1941-1 (September 1965).

32. Page, W.A. and Arnold, J.O., "Shock Layer Radiation of Blunt
    Bodies at Re-entry Velocities", NASA TR-R-193 (April 1964).

33. Hoshizaki, H., "Equilibrium Total Radiation Measurements in Air
    at Superorbital Entry Velocities", Lockheed Missiles and Space Co.,
    Report No. 6-90-63-97 (October 1963).

34. Nerem, R.M. and Stickford, G.H., "Shock Tube Studies of Equilibrium
    Air Radiation", AIAA J. 3, 1011-1018 (1965).

35. Diaconis, N.S., Warren, W.R. and Shaw, T.E., "The Hypervelocity
    Heat Protection Problem", Presented at XVI International Astronautical
    Congress, Athens, Greece (September 1965). Also General Electric Co.,
    Report TIS R65SD60 (November 1965).
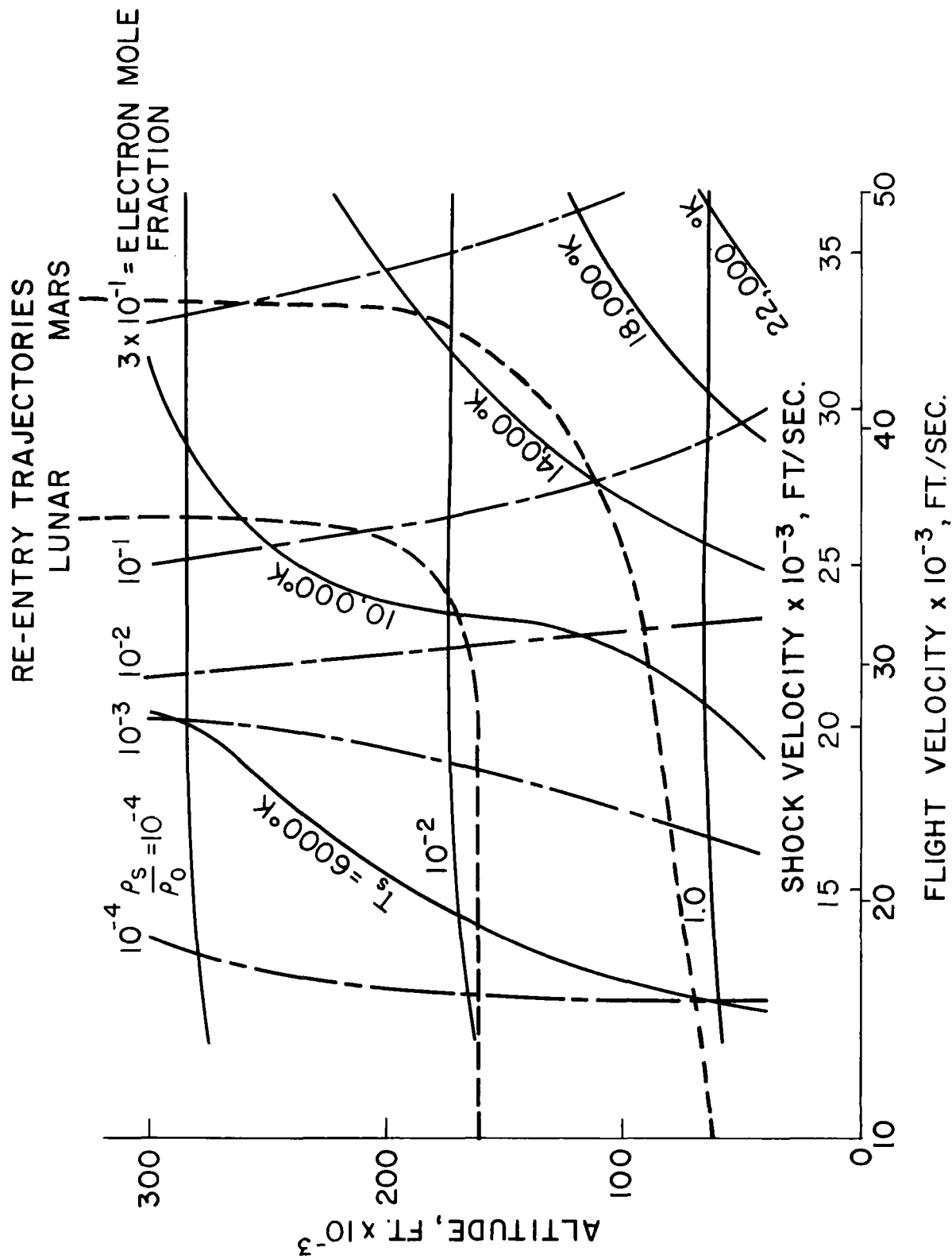
Figure 1. 1 – Blunt body stagnation point equilibrium gas properties for entry into earth atmosphere.
Shock velocity indicates model stagnation region simulation in shock tube flow.
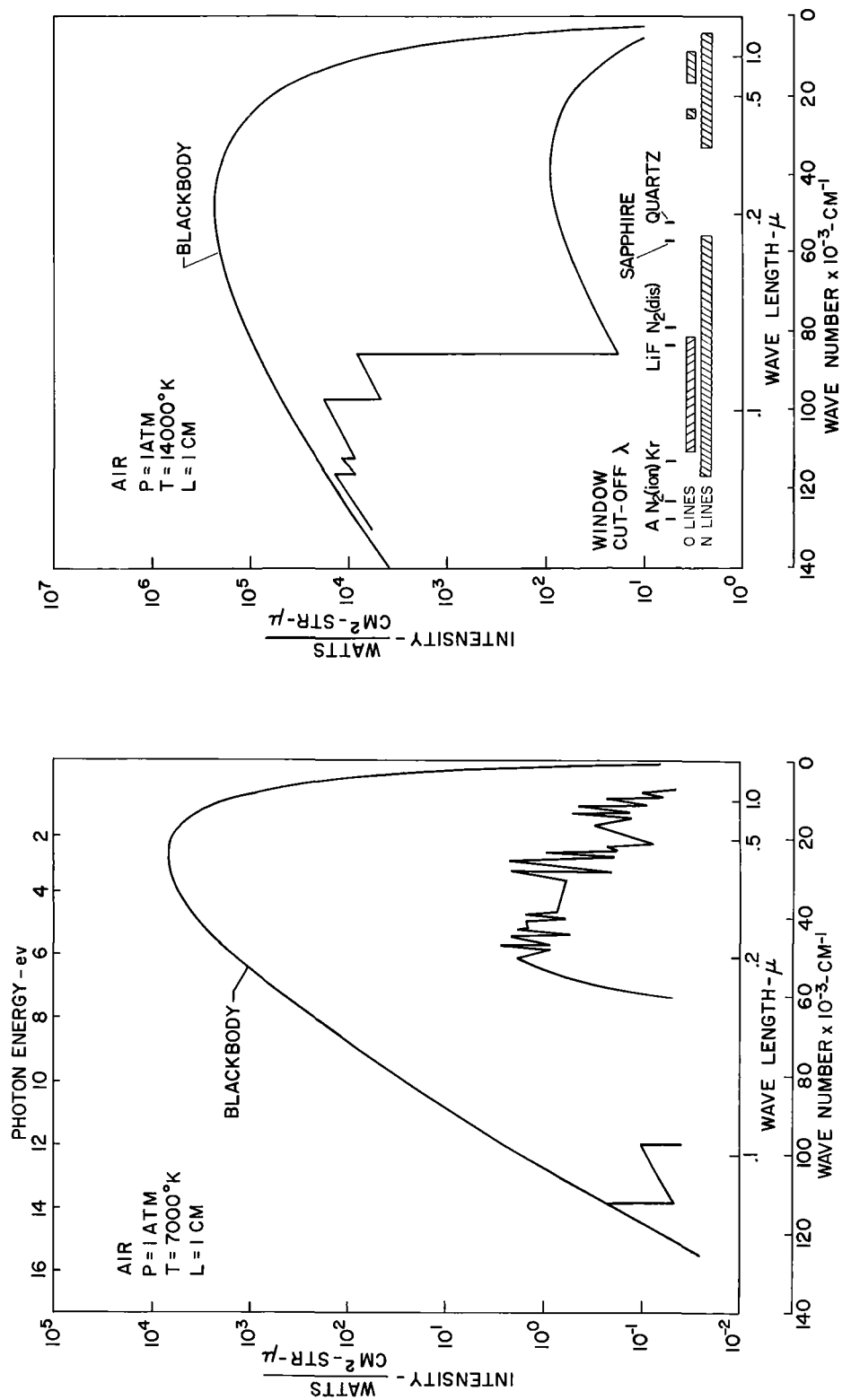
Figure 1.2 – Wavelength and temperature dependence of air radiation. Line radiation is not shown. Approximate short wavelength cut-off values for several solid and gaseous window materials are indicated.
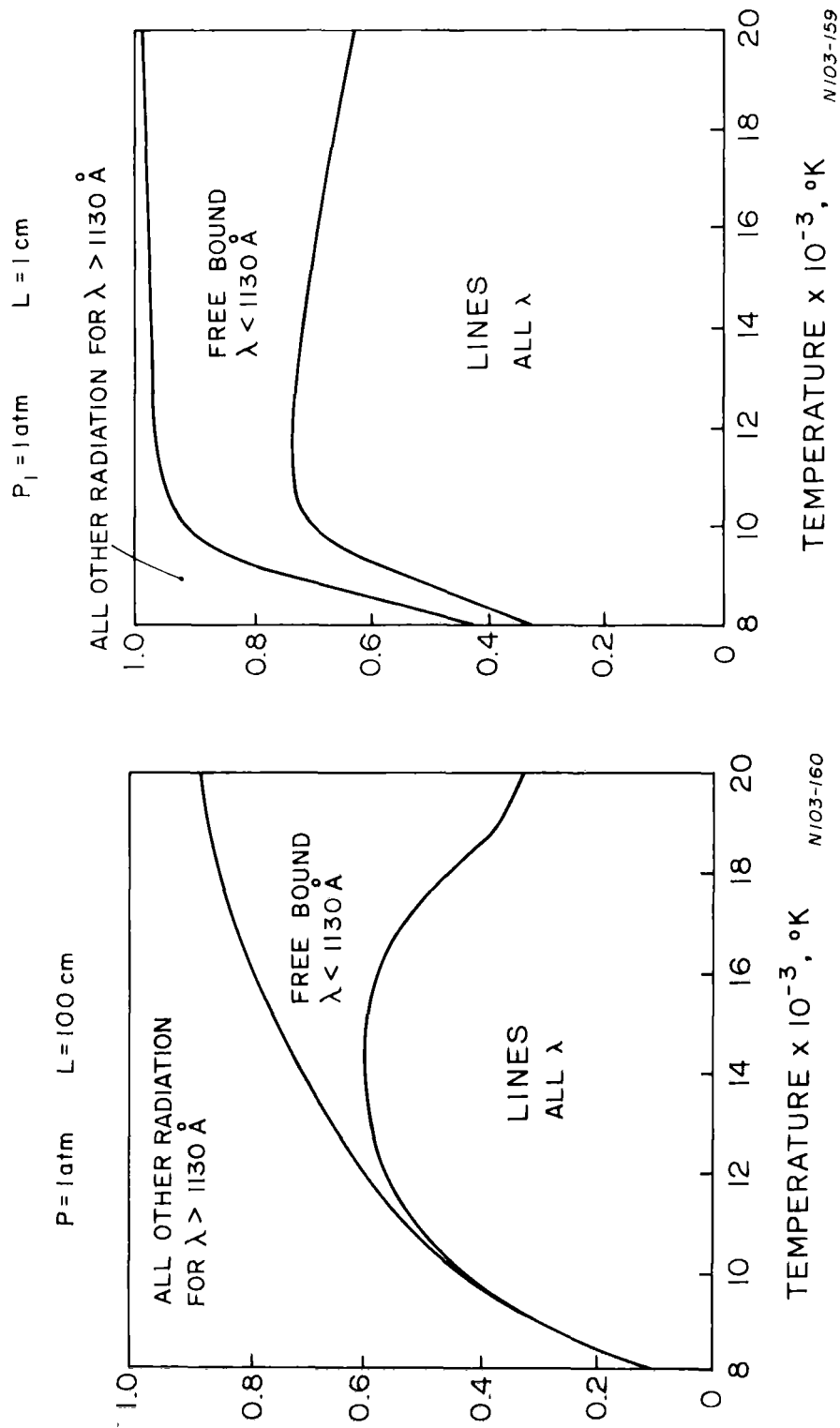
Figure 2.1 – Contribution of various radiating systems in nitrogen plasma taken from Ref. 4.
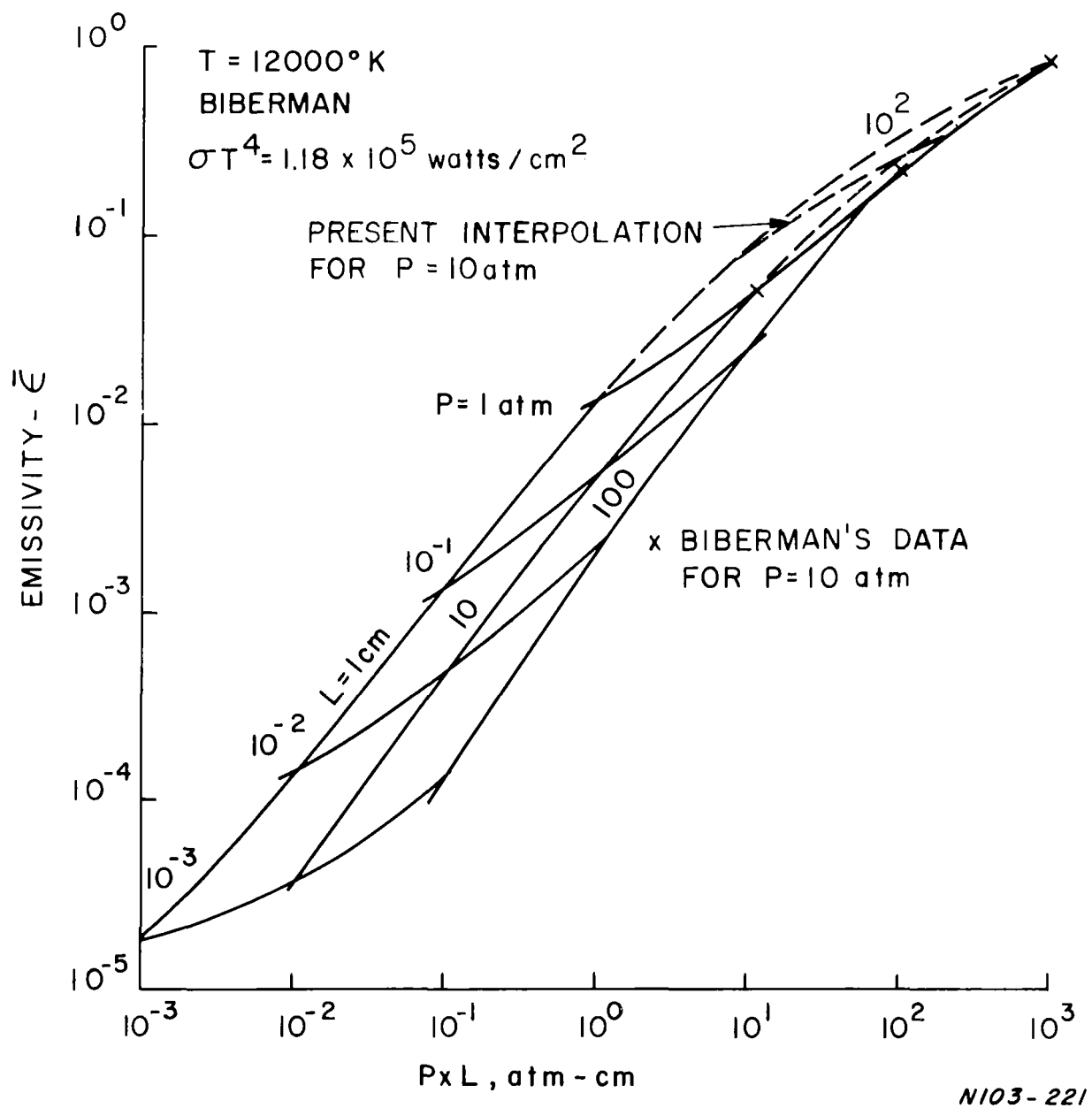
Figure 2.2 - Emissivity of air as a function of pressure and gas layer thickness at T = 12,000°K.
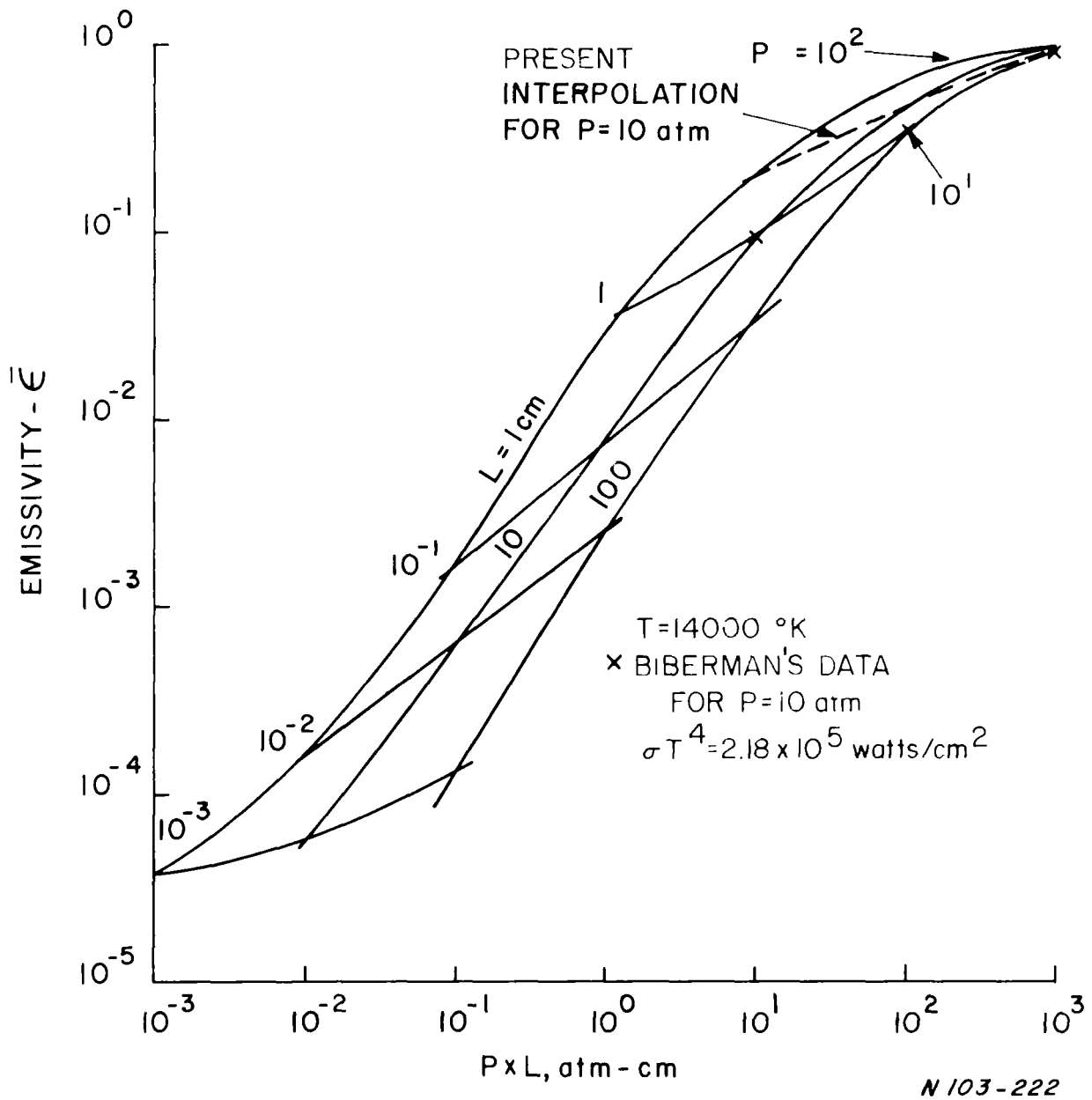
Figure 2.3 - Emissivity of air as a function of pressure and gas layer thickness at T = 14,000°K.
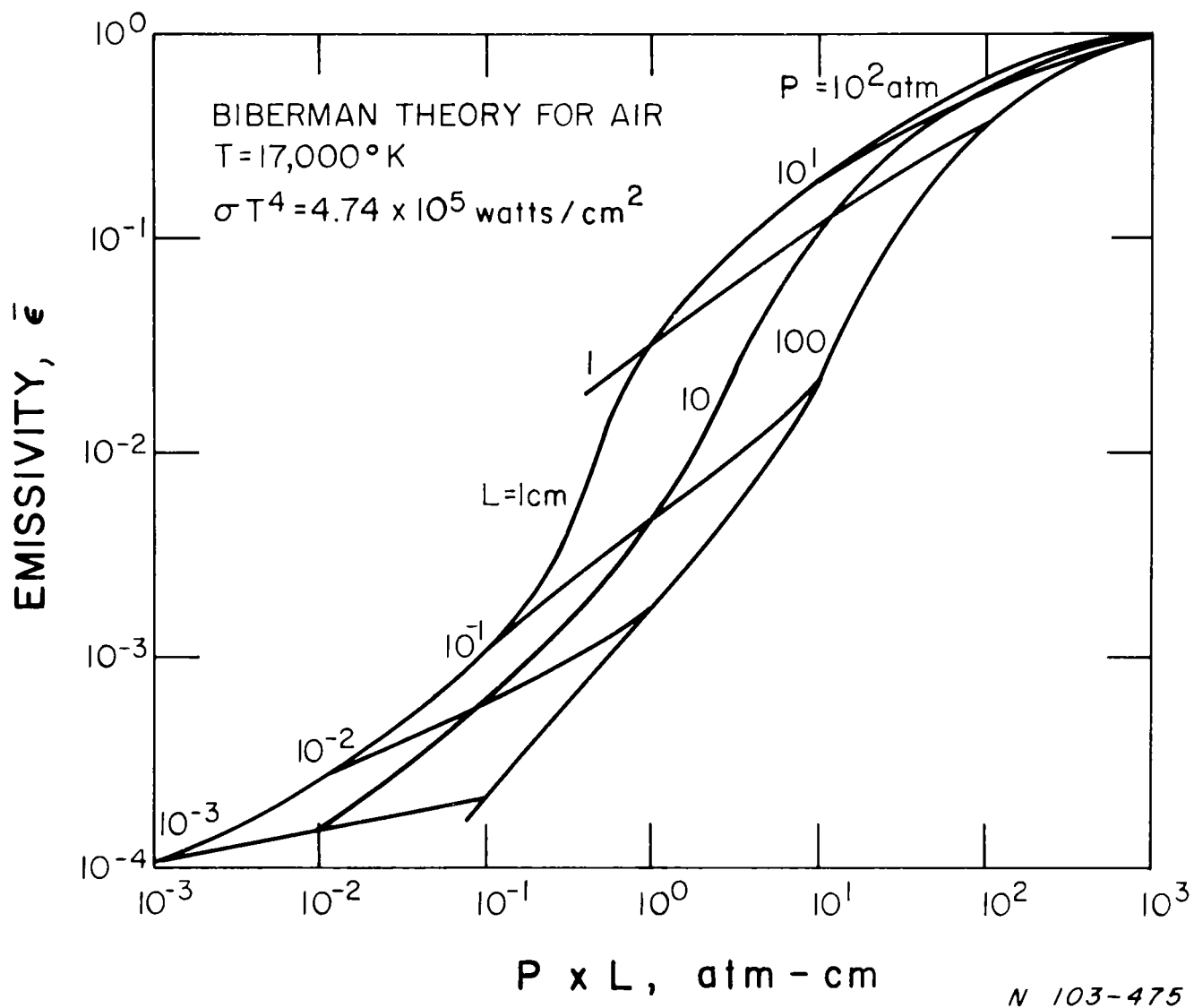
Figure 2.4 - Emissivity of air as a function of pressure and gas layer thickness at T = 17,000°K.
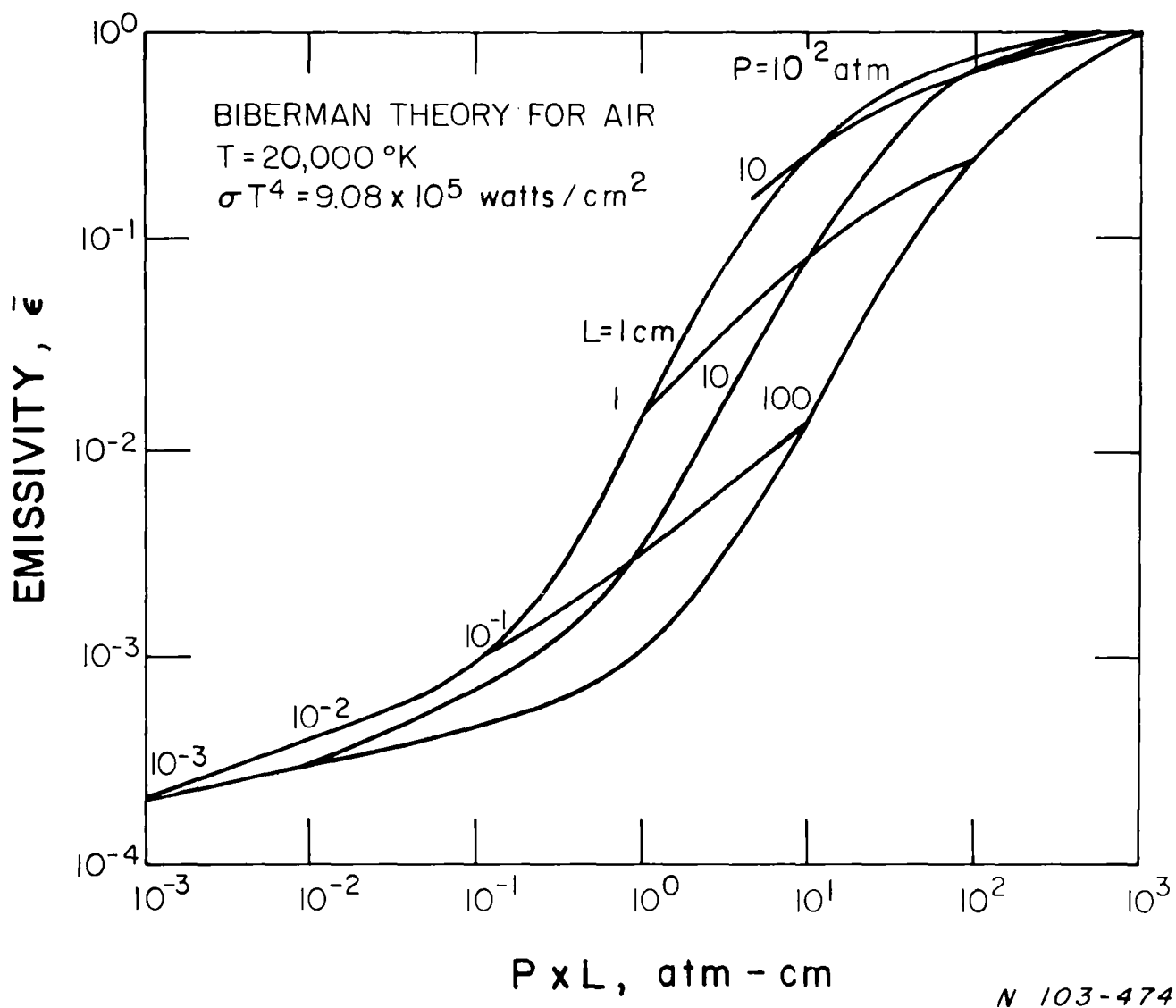
Figure 2.5 - Emissivity of air as a function of pressure and gas layer thickness at T = 20,000°K.
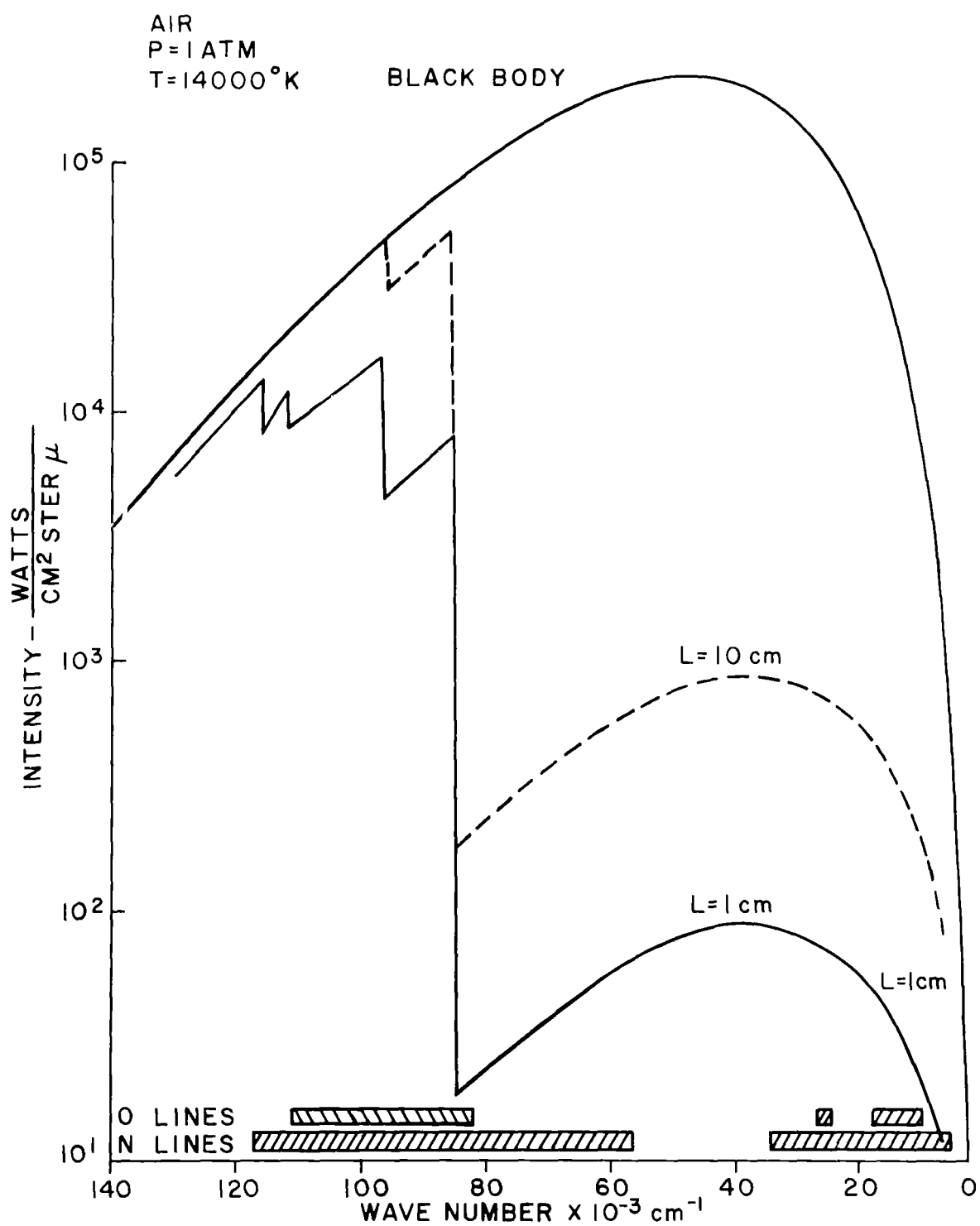
Figure 2.6 - The effect of gas thickness on the spectral intensity of continuum radiation in air. Data taken from Ref. 3 with indicated location of atomic lines.
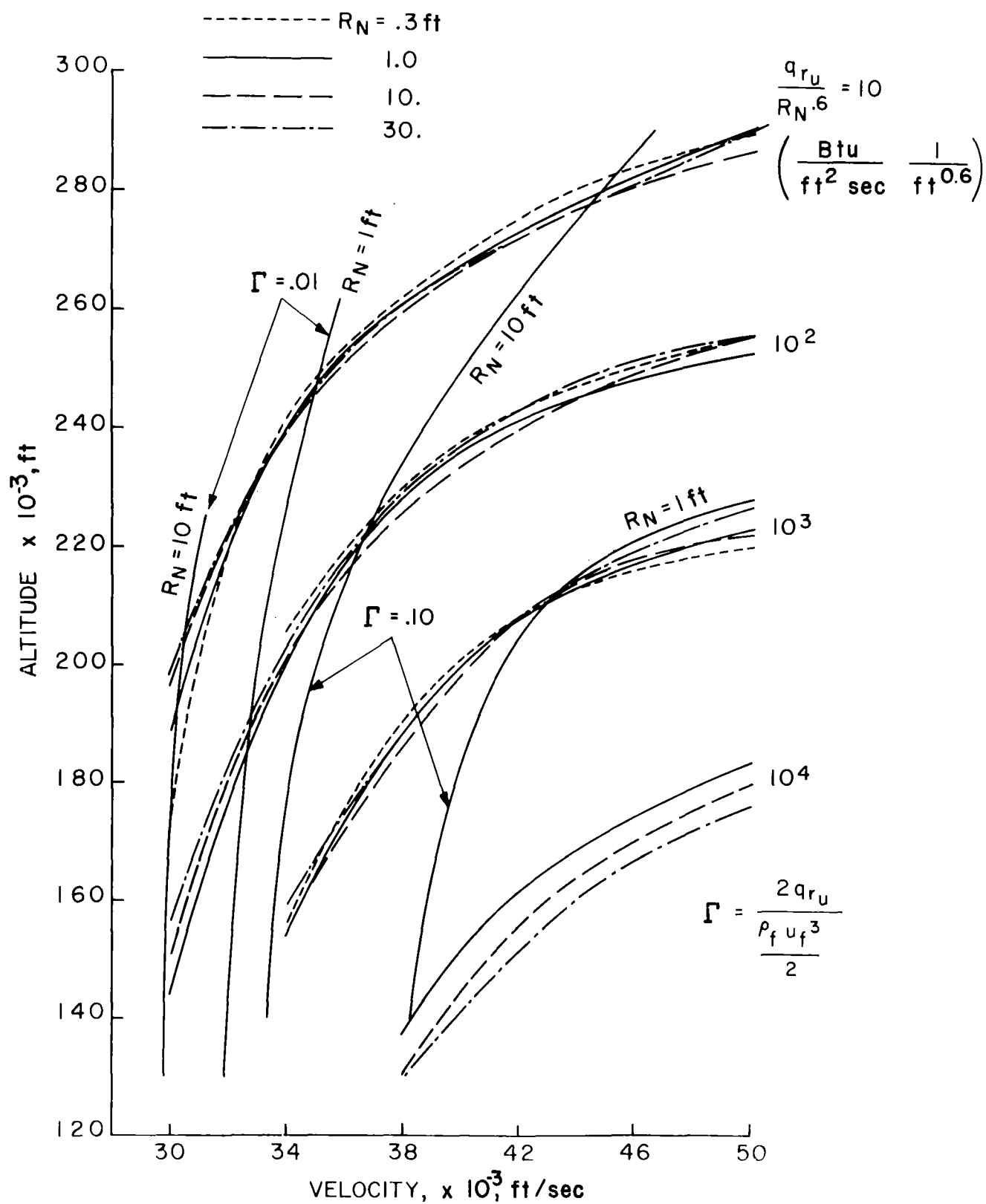
Figure 2.7 - Correlation of the Biberman, et al predictions of uncoupled stagnation point radiative heating for a range of body nose radii.
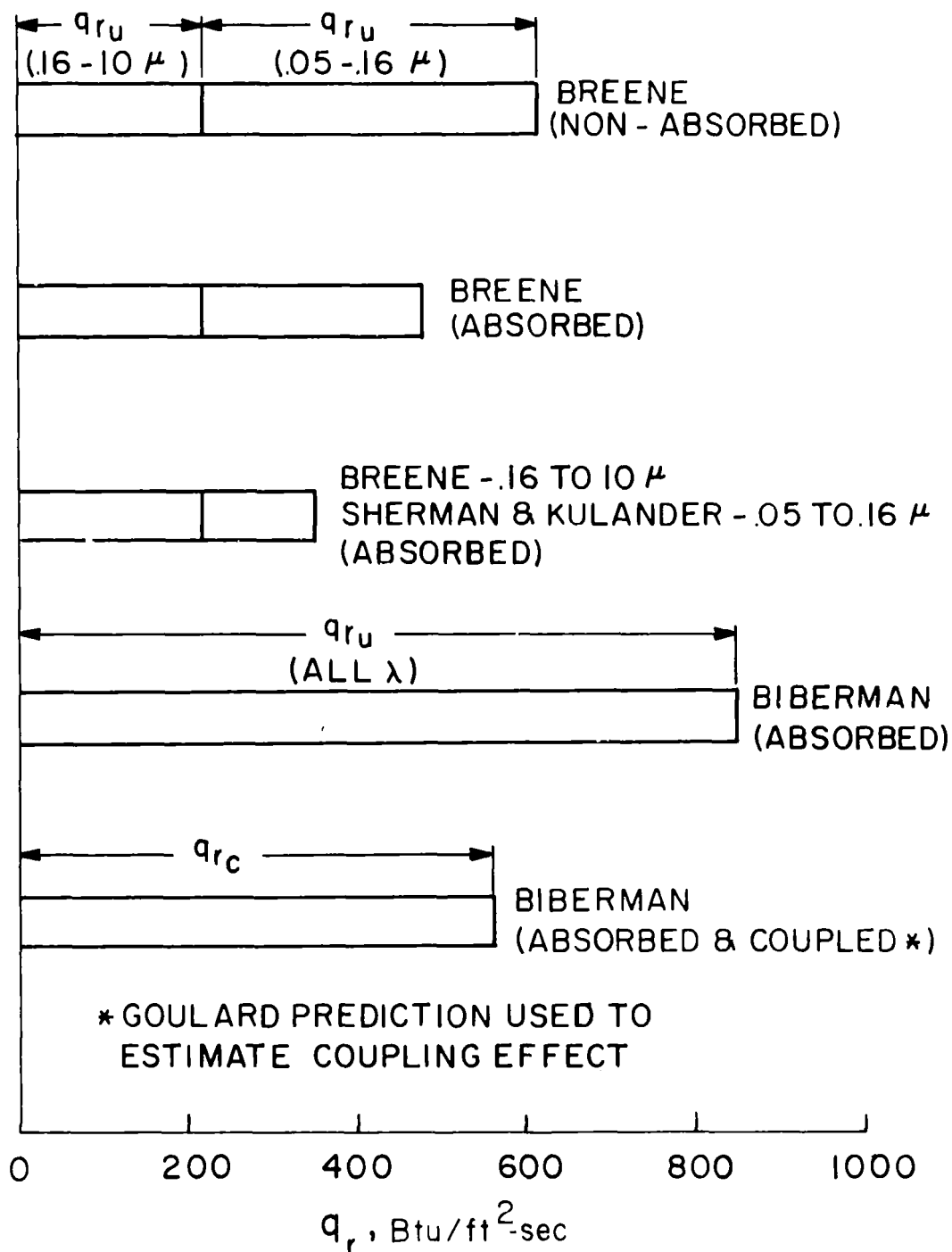
Figure 2. 8 - Comparison of the radiative heating predictions of several investigators indicating the effects of self-absorption and coupling.
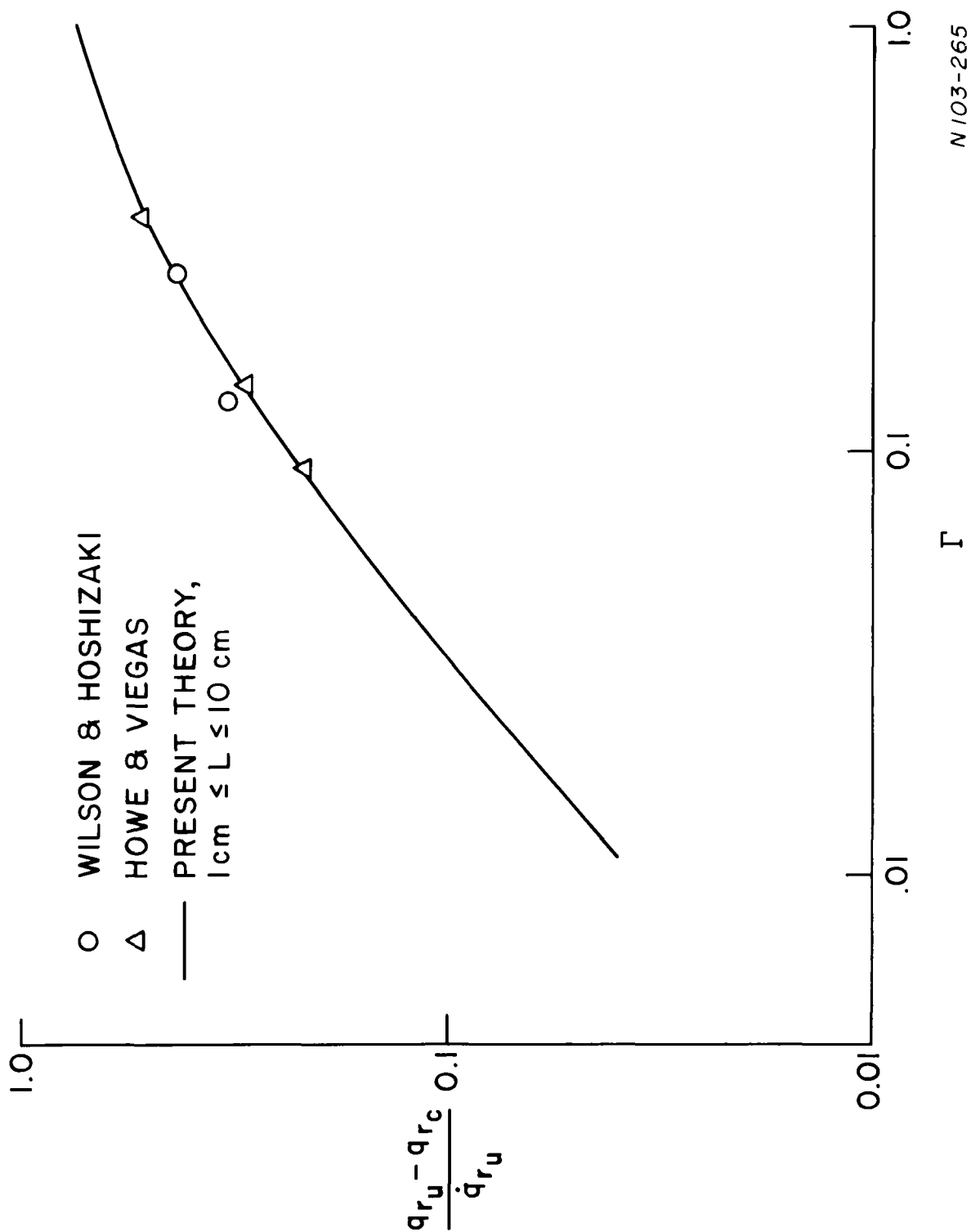
Figure 2.9 – Effect of coupling parameter on reduction of radiative heat transfer based on isothermal shock layer assumption.

N103-265
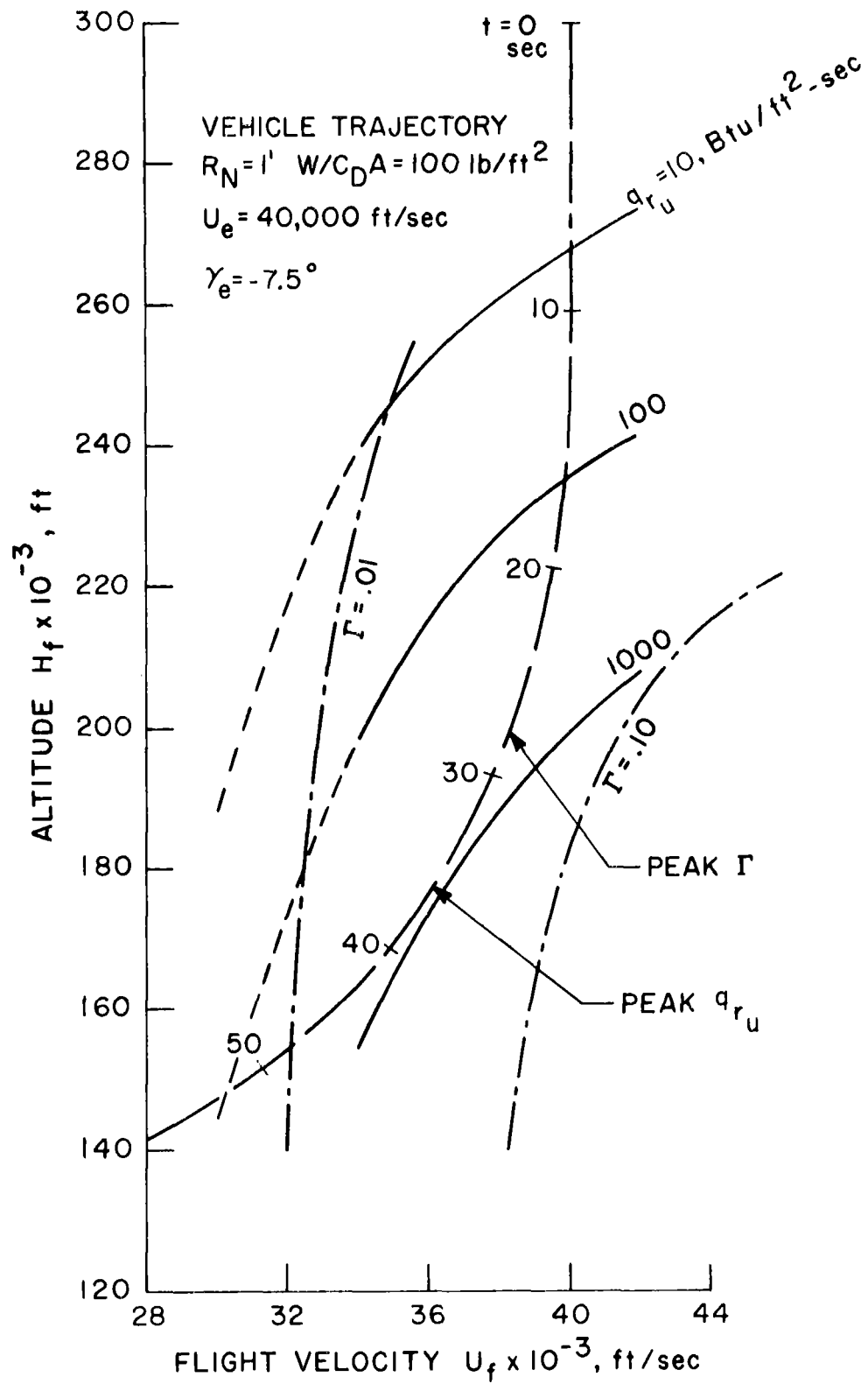
Figure 2.10 - Re-entry vehicle trajectory showing positions of peak uncoupled stagnation point radiative heating and peak coupling parameter (Biberman et al predictions).
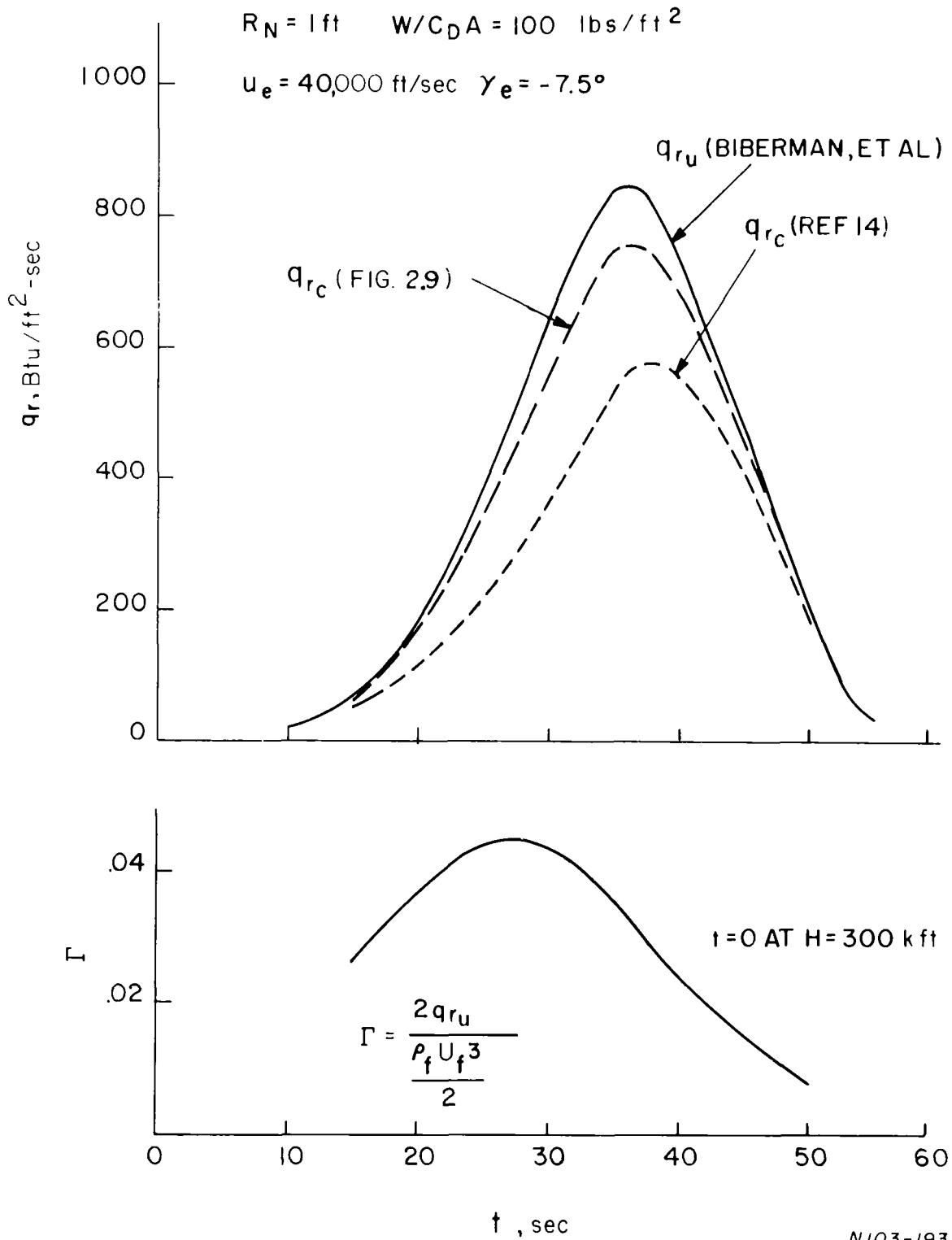
Figure 2.11 - Variation of uncoupled radiative heat transfer, q_{r_u}, and coupling parameter, for vehicle trajectory on Fig. 2.10. Reductions in radiative heating, as predicted by three approximate analyses, are shown.

PLASTIC LINER

ELECTRODES

POWER
COLLECTOR COLLAR

DRIVER TUBE
4 1/2' LONG | MAXIMUM
3" ID | DIMENSION

DRIVEN TUBE
31.5' LONG
6" ID

304 KILOJOULE
POWER SUPPLY
380 μf
40 KV
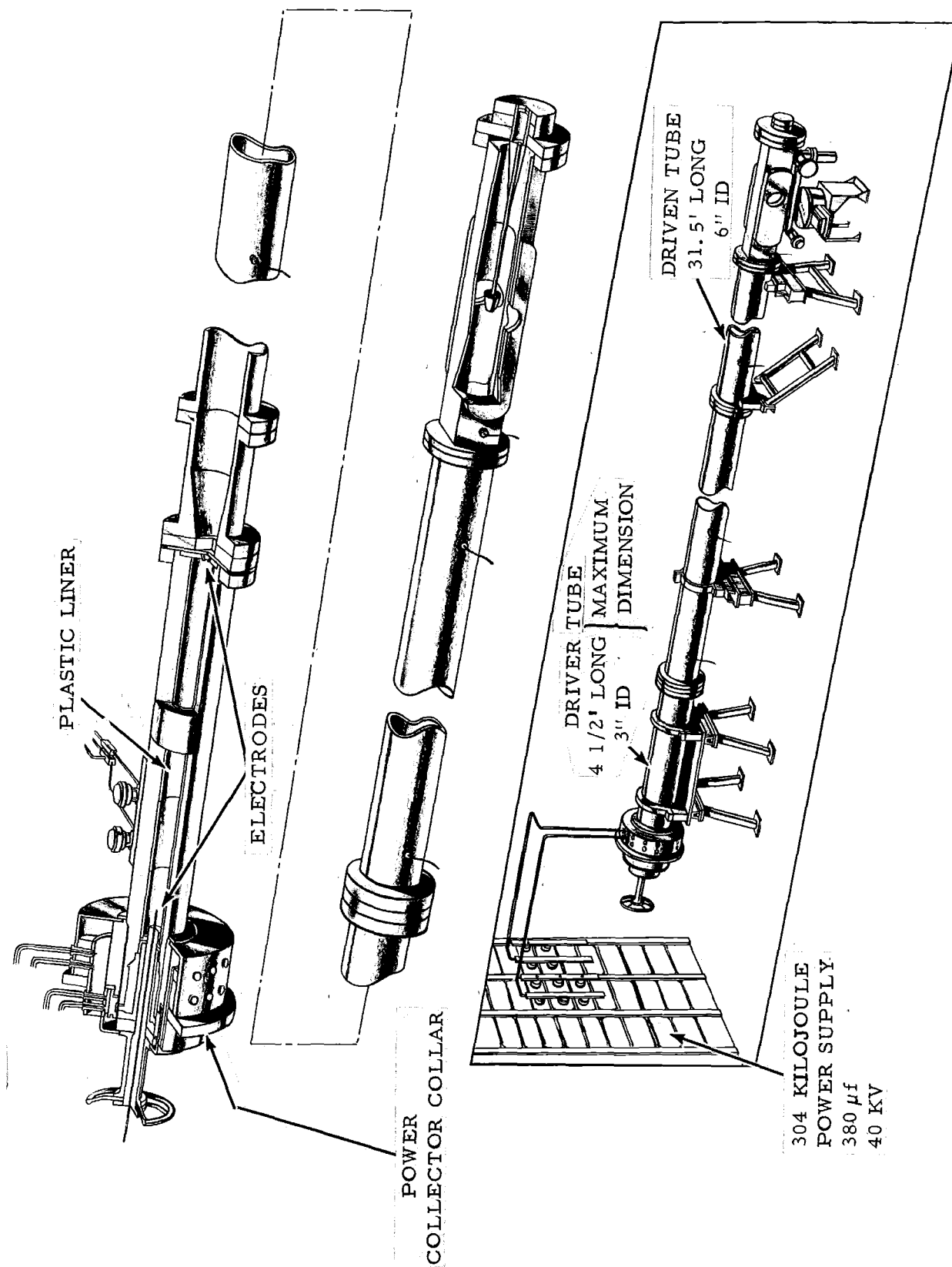
Figure 3.1 – Electrically driven shock tube.
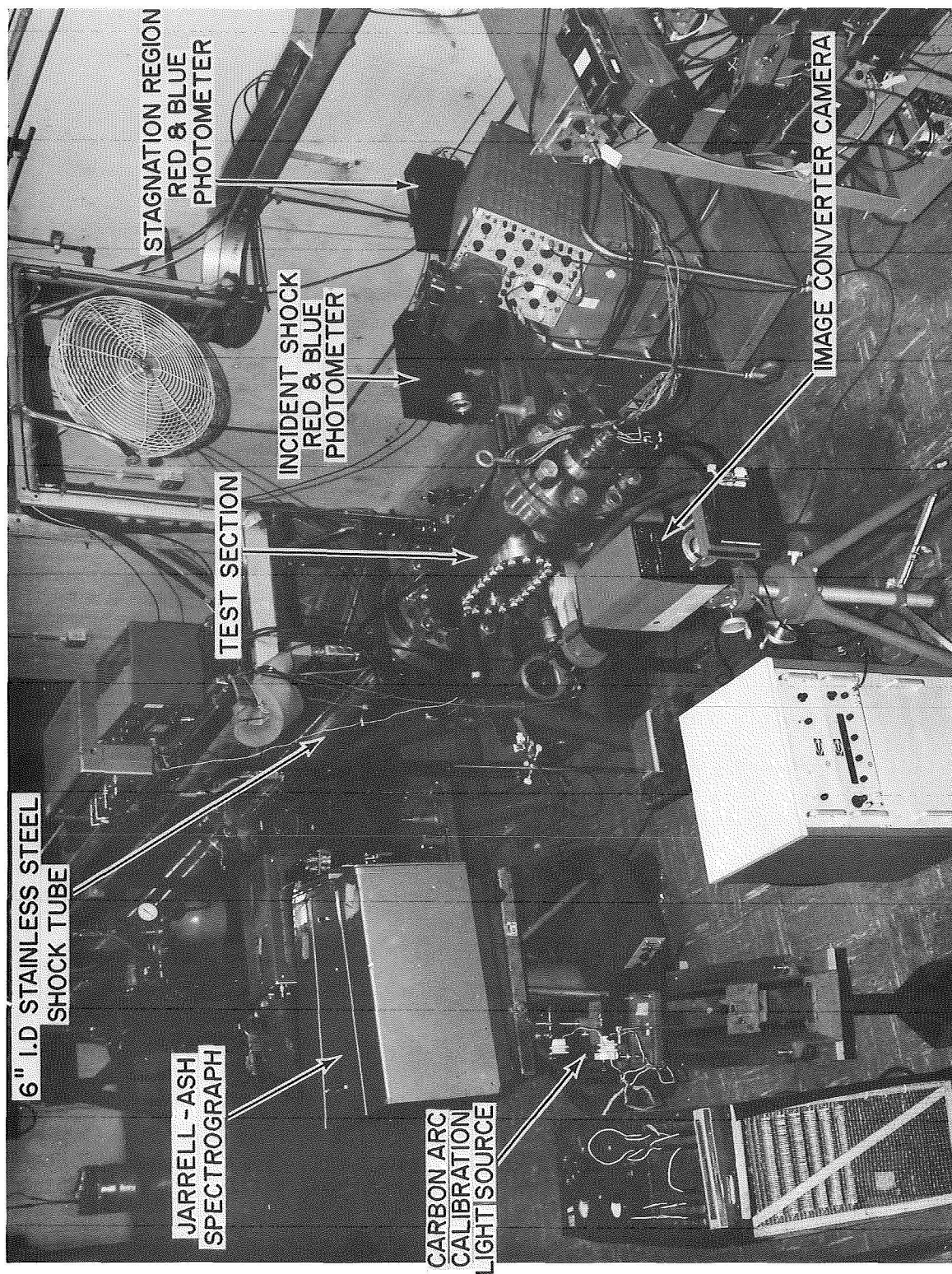
Figure 3.2 – Test section end of driven tube.

STAGNATION REGION
RED & BLUE PHOTOMETER

INCIDENT SHOCK
RED & BLUE PHOTOMETER

TEST SECTION

IMAGE CONVERTER CAMERA

6" I.D STAINLESS STEEL
SHOCK TUBE

JARRELL-ASH SPECTROGRAPH

CARBON ARC
CALIBRATION
LIGHT SOURCE

-68-
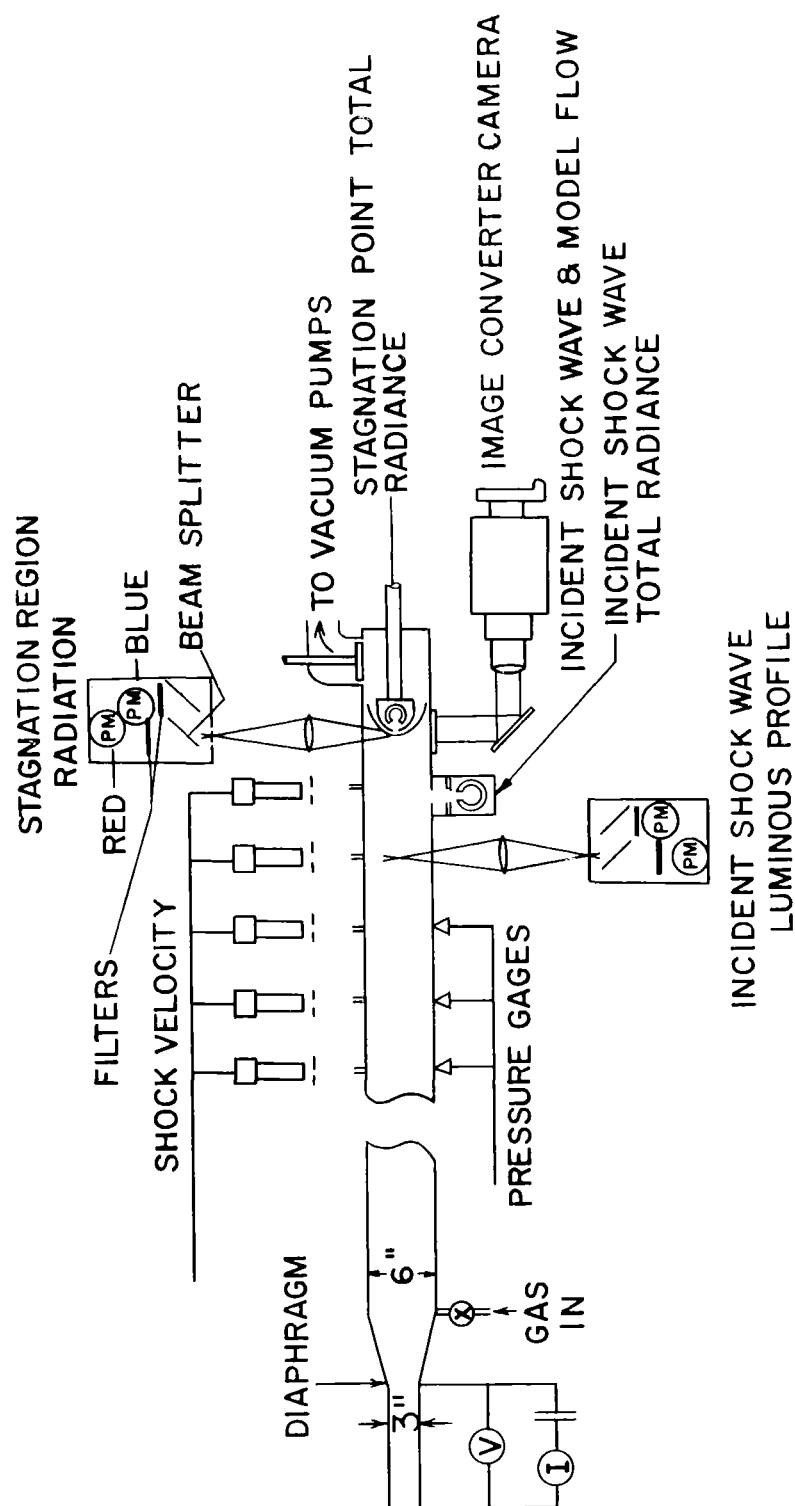
Figure 3.3 – Schematic diagram of instrumentation for study of gas radiance and for determining shock tube performance.
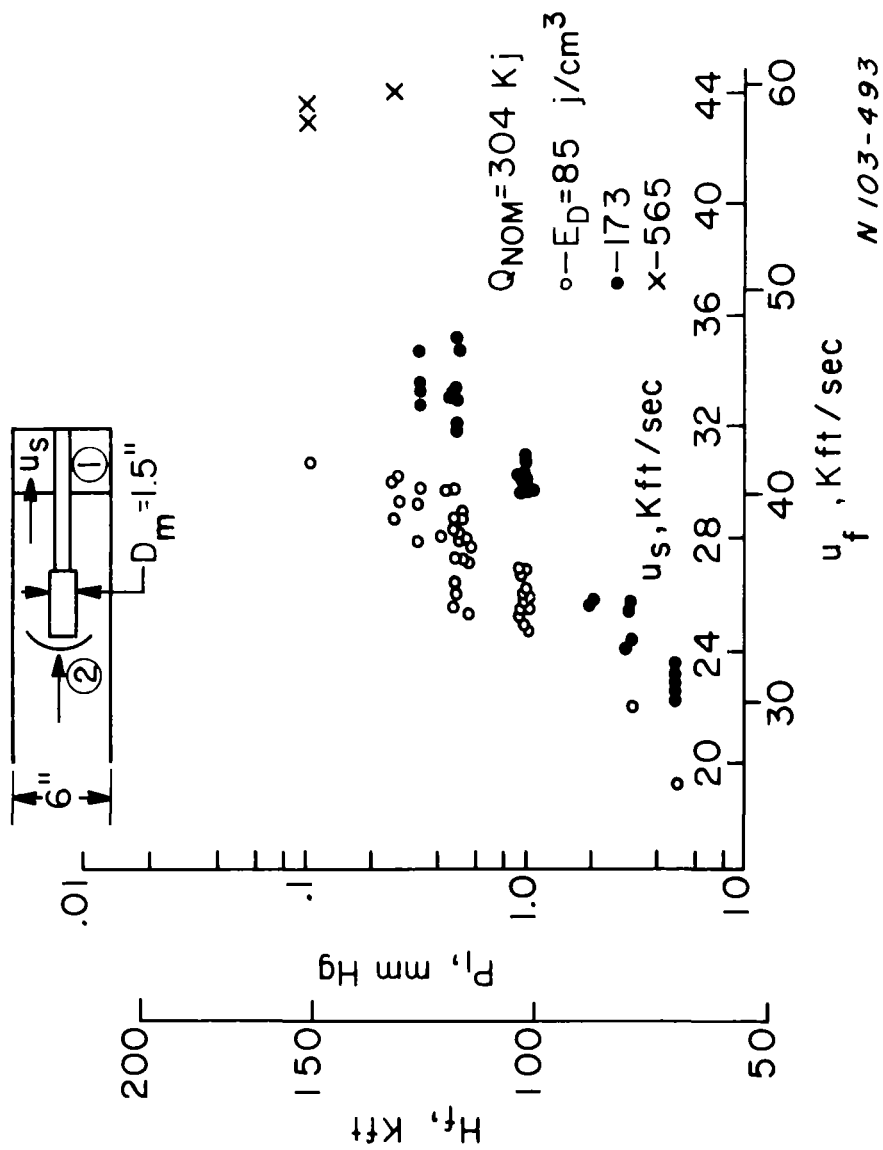
Figure 3.4 – Shock velocity-initial pressure performance for electrically driven shock tube showing representative data for three different driver geometries, specified by nominal driver gas energy density, E_D.
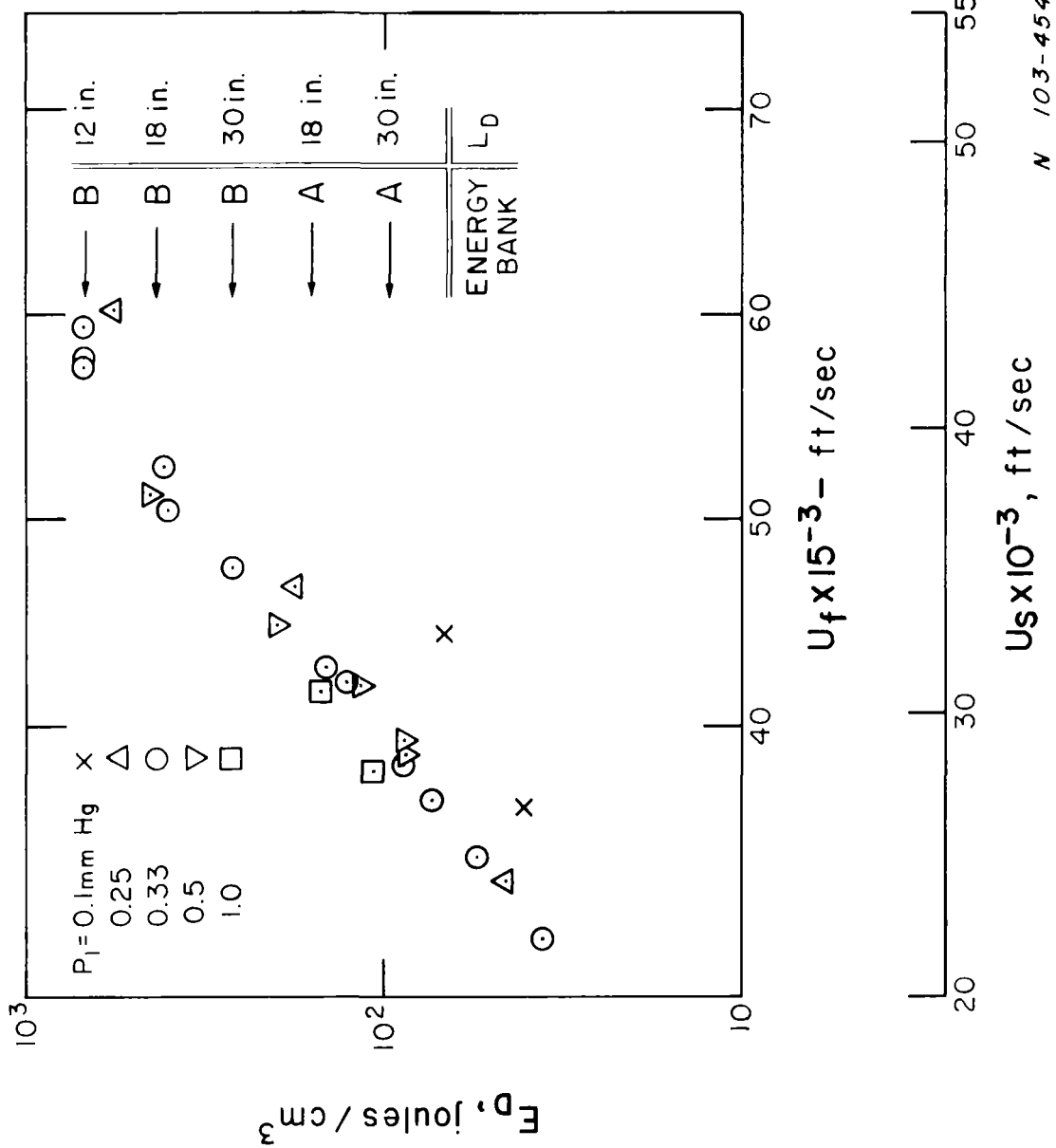
Figure 3.5 – Shock tube performance as a function of driver energy density. Range of operation with the available energy storage banks is indicated.
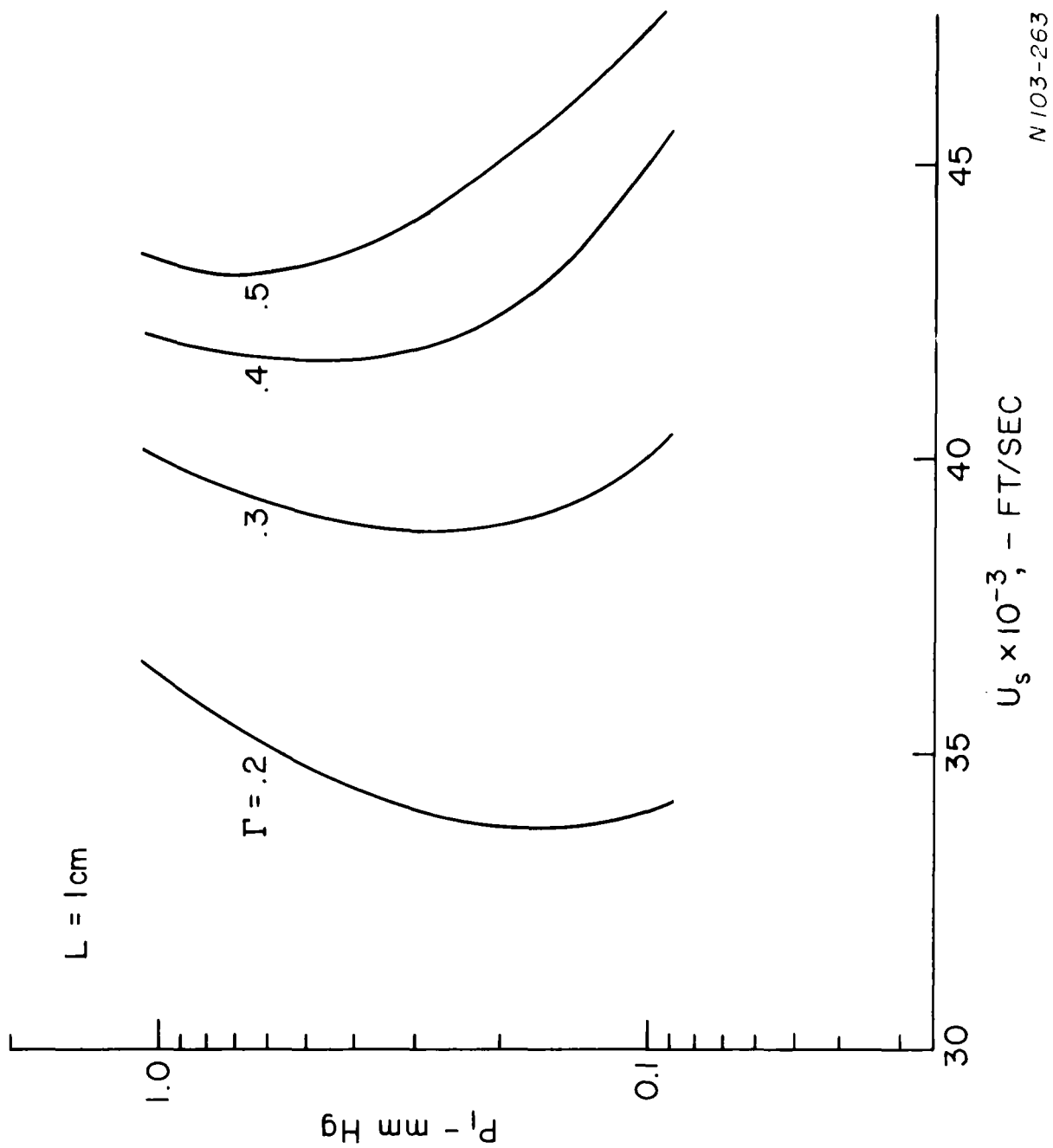
Figure 3.6 - Radiative transfer coupling parameter, Γ, as a function of shock velocity for stand-off distance of $L = 1$ cm.

N103-263
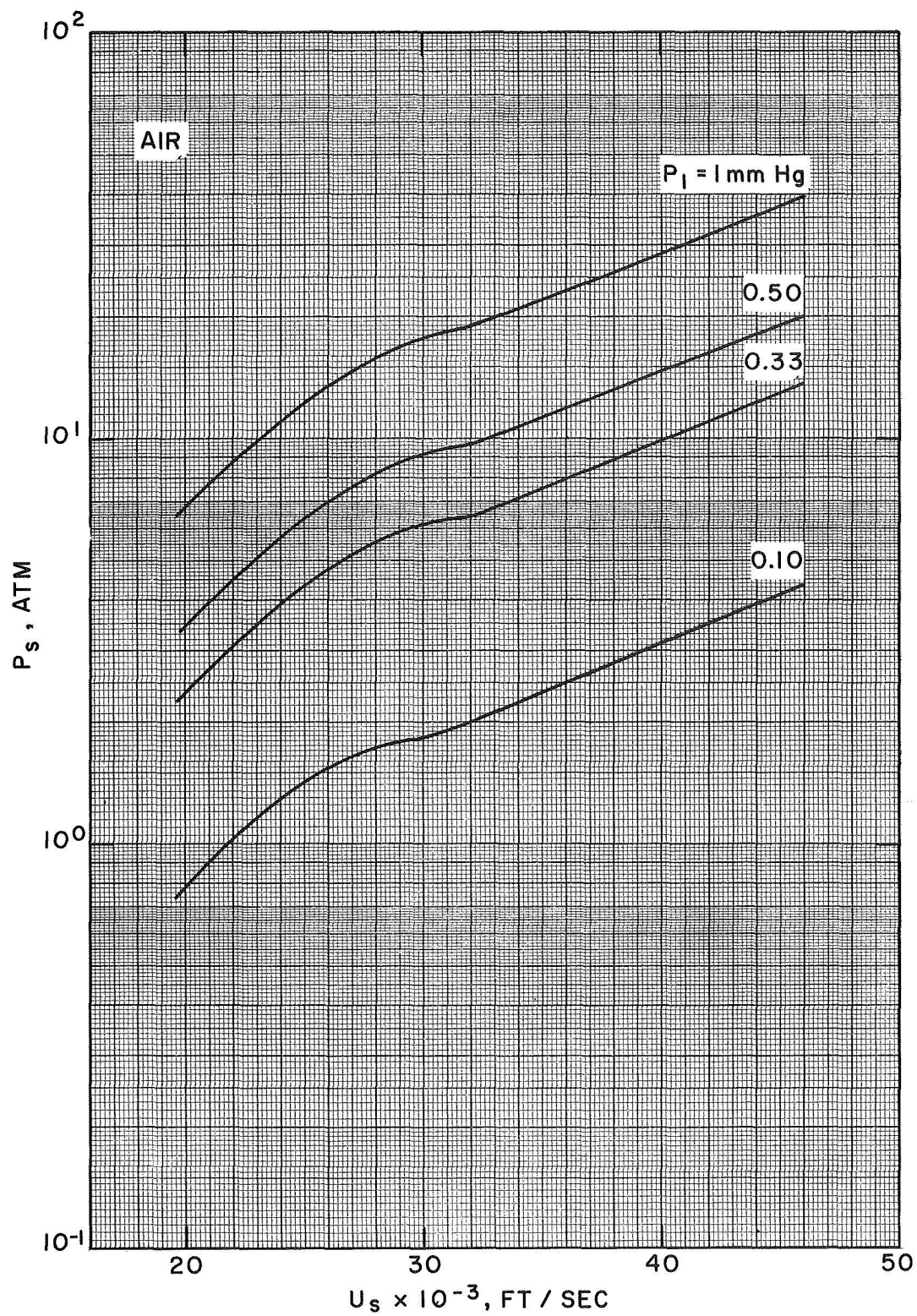
Figure 3.7 - Blunt model stagnation pressure as a function of shock velocity in a shock tube flow.
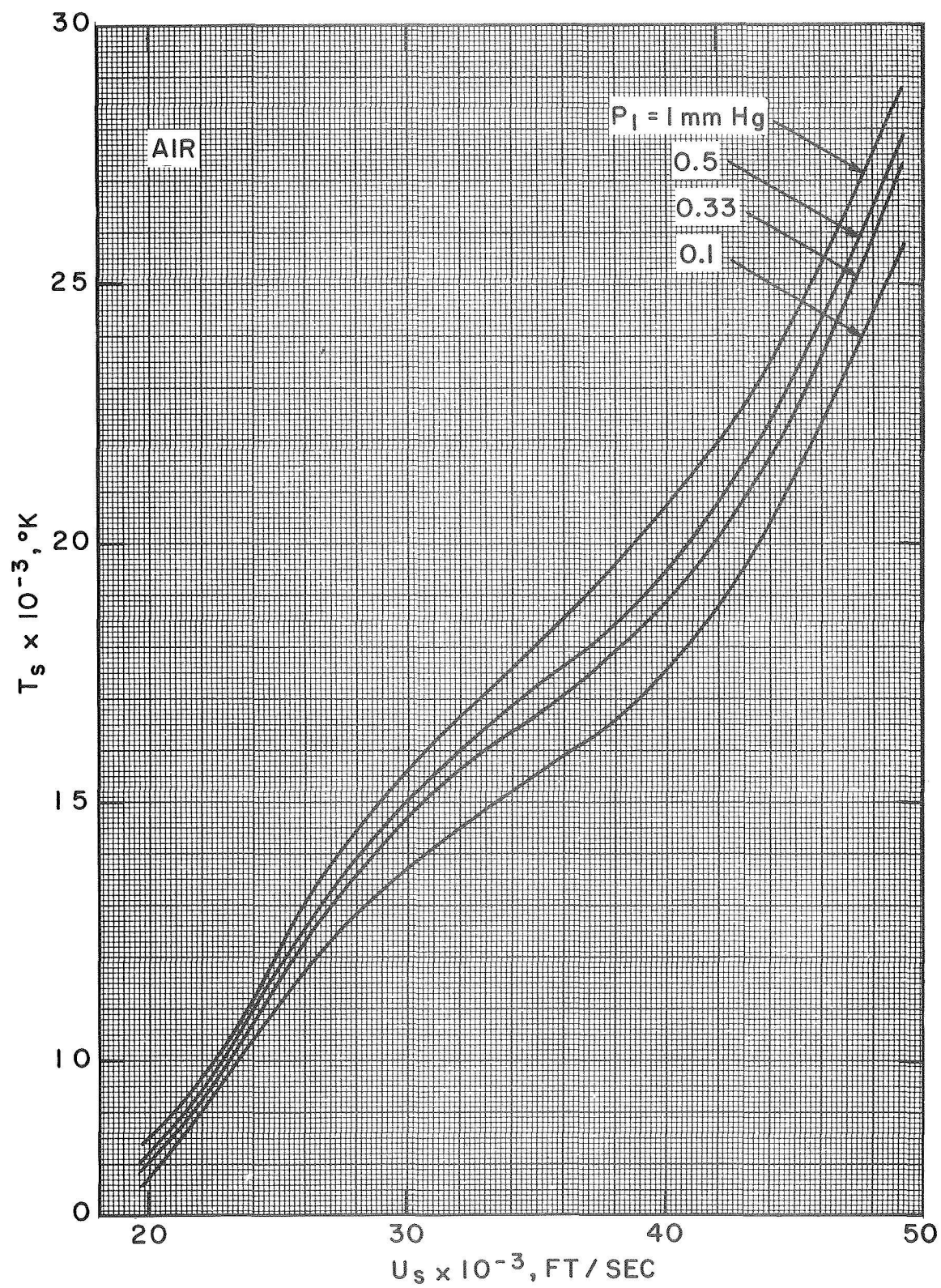
Figure 3.8 - Blunt model stagnation temperature as a function of shock velocity in a shock tube flow.
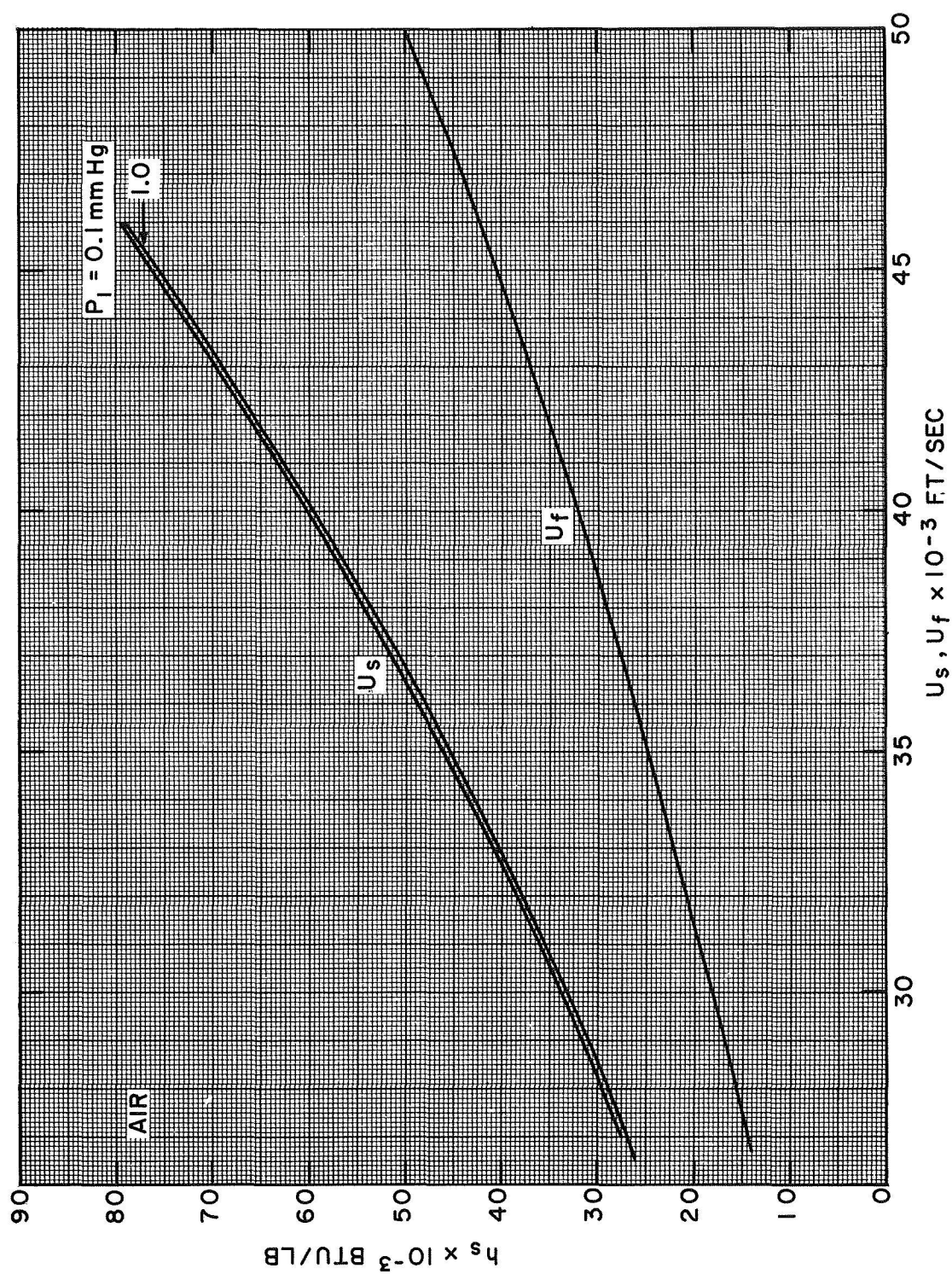
Figure 3.9 – Correspondence between shock tube and flight conditions for stagnation enthalpy simulation.

THIN PLATINUM FILM

$\dot{q}_r$

QUARTZ
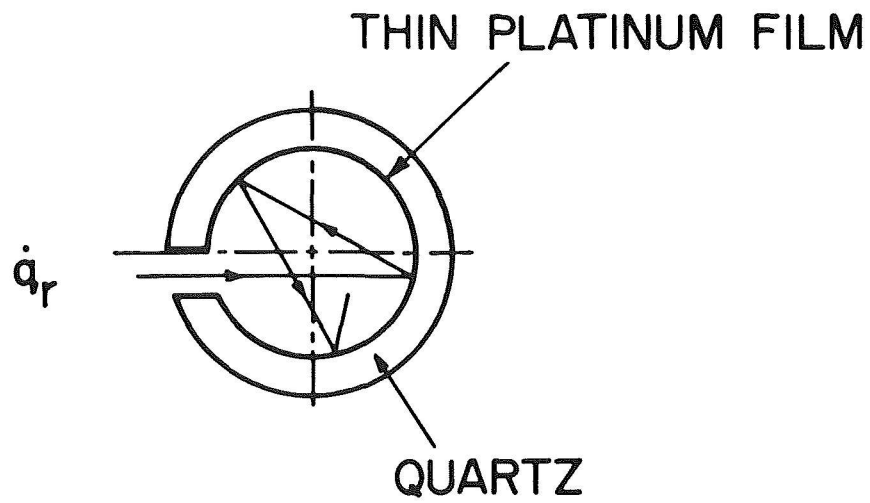
Figure 3.10 - Geometry of the cavity gage.

ENTRANCE SLIT
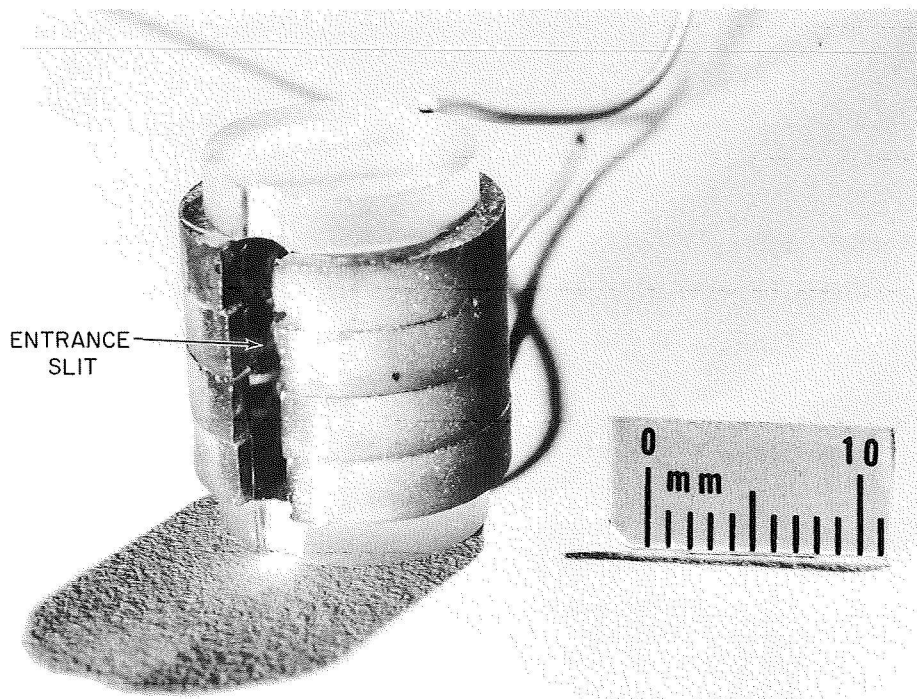
Figure 3.11 - Total radiation cavity gage.
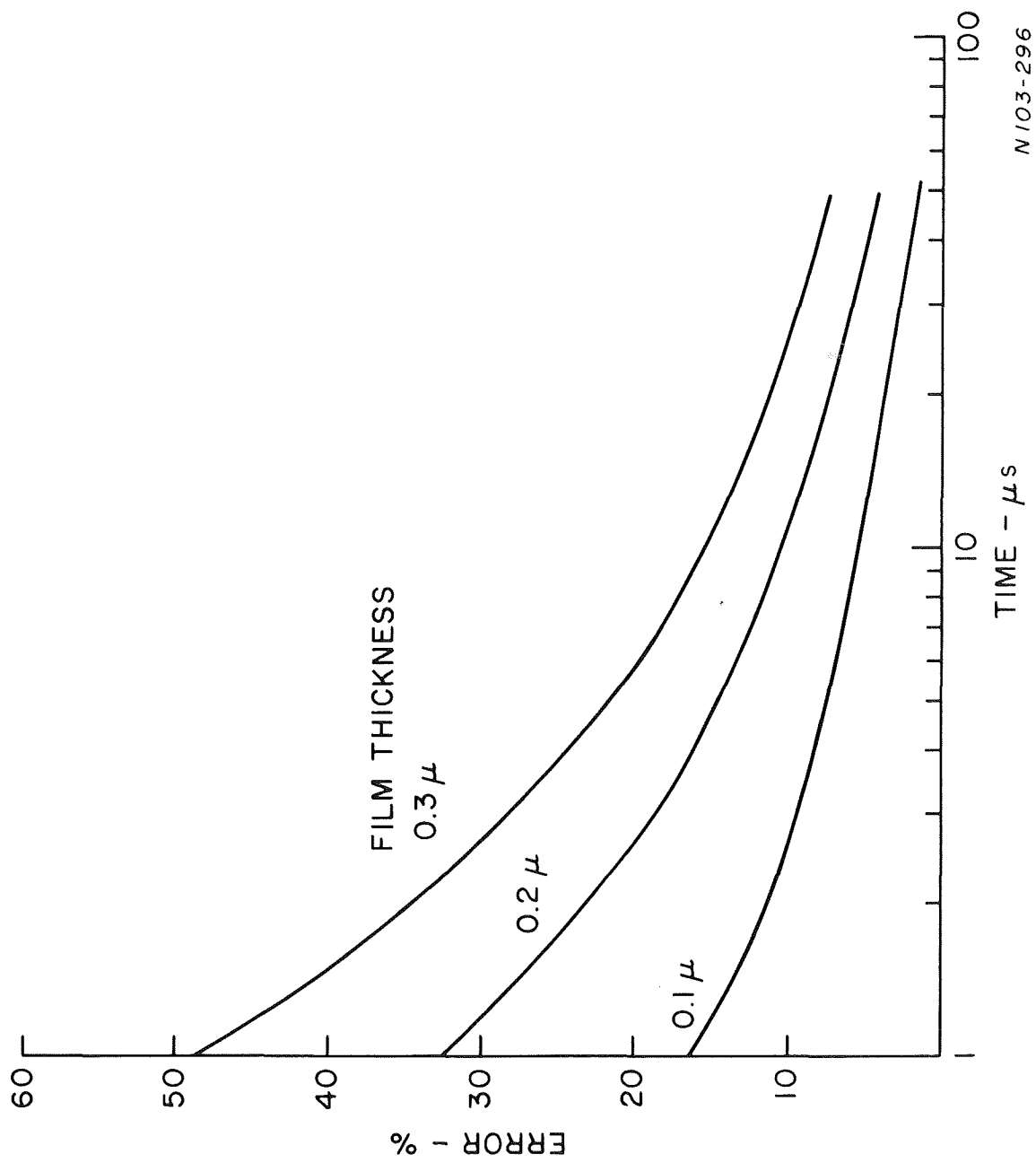
Figure 3.12 - Thin film thermometer error due to finite thickness of the film.
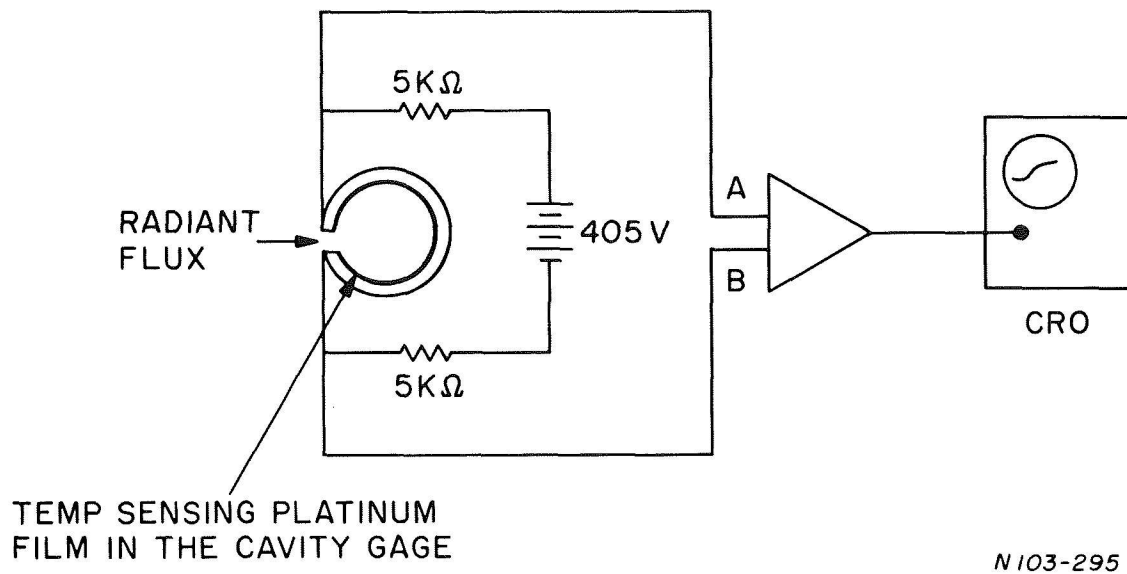
Figure 3.13 - Schematic of the gage electric circuit.
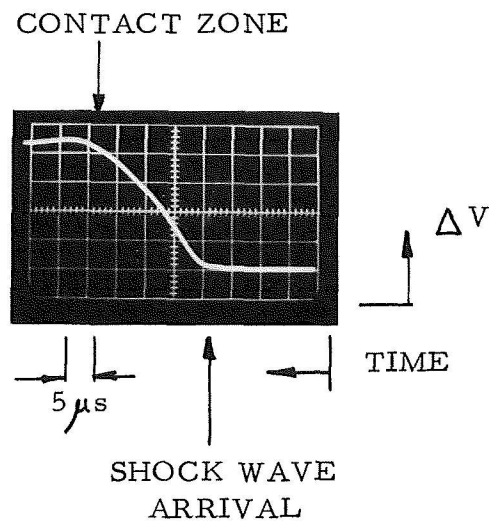
Figure 3.14 - Typical oscilloscope trace of a cavity gage signal.
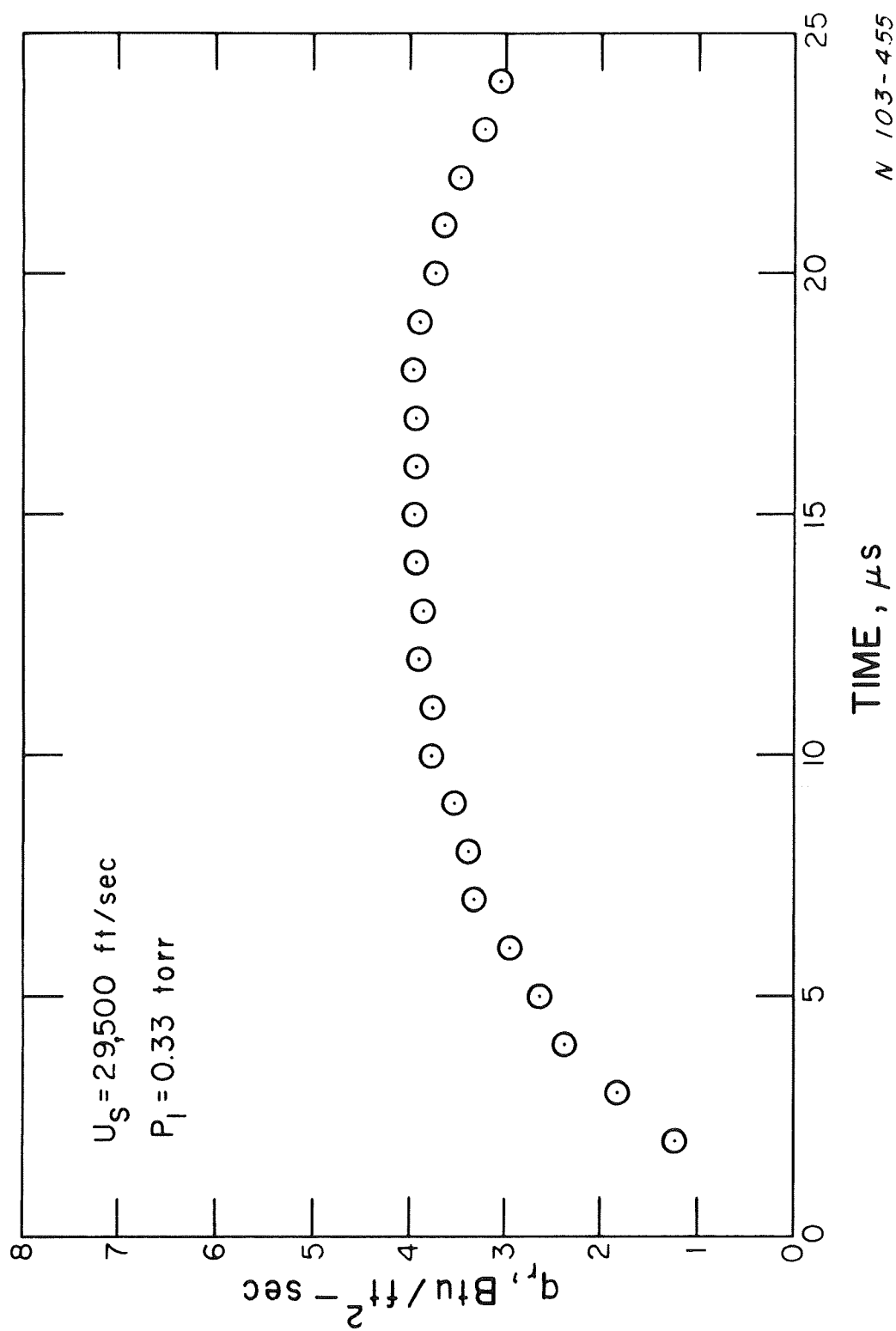
Figure 3.15 - Heat transfer rate obtained with the help of Eq. (3.1) for the gage output in Fig. 3.14.

COPPER SHIELD

CAVITY GAGE

1.5" dia.

LEXAN MODEL

GAGE HOLDER

BOW SHOCK
WAVE
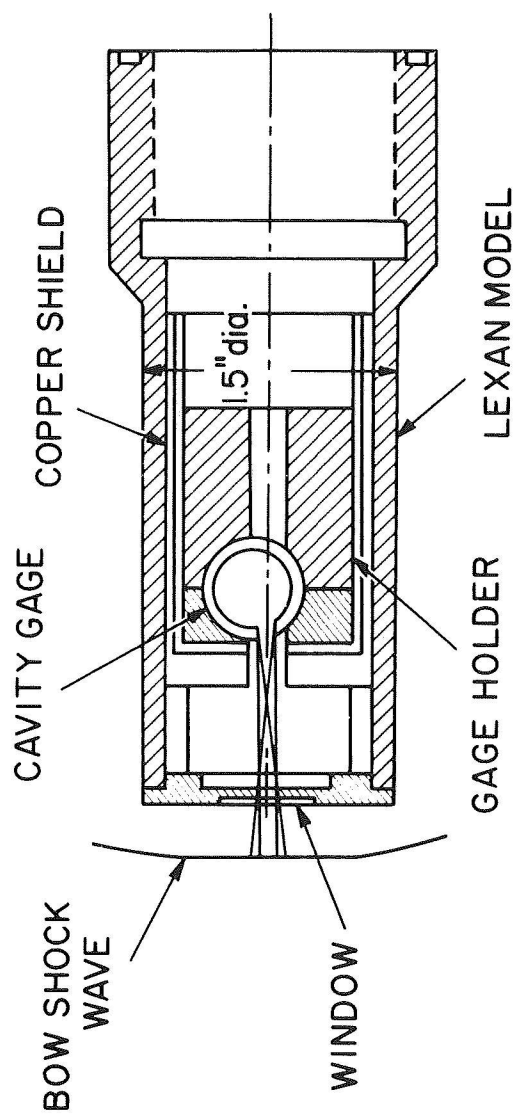
WINDOW

N103-298

Figure 3.16 – Total radiation cavity gage model with solid windows used for radiation measurements.

V

TIME → ARRIVAL OF SHOCK WAVE

$P_I = 0.33$ mm Hg $U_S = 31000$ ft/sec.

→ ⊢ 5 μ sec.

CAVITY GAGE WITH LiF WINDOW

MODEL GAS A AT 2 ATM PRESSURE
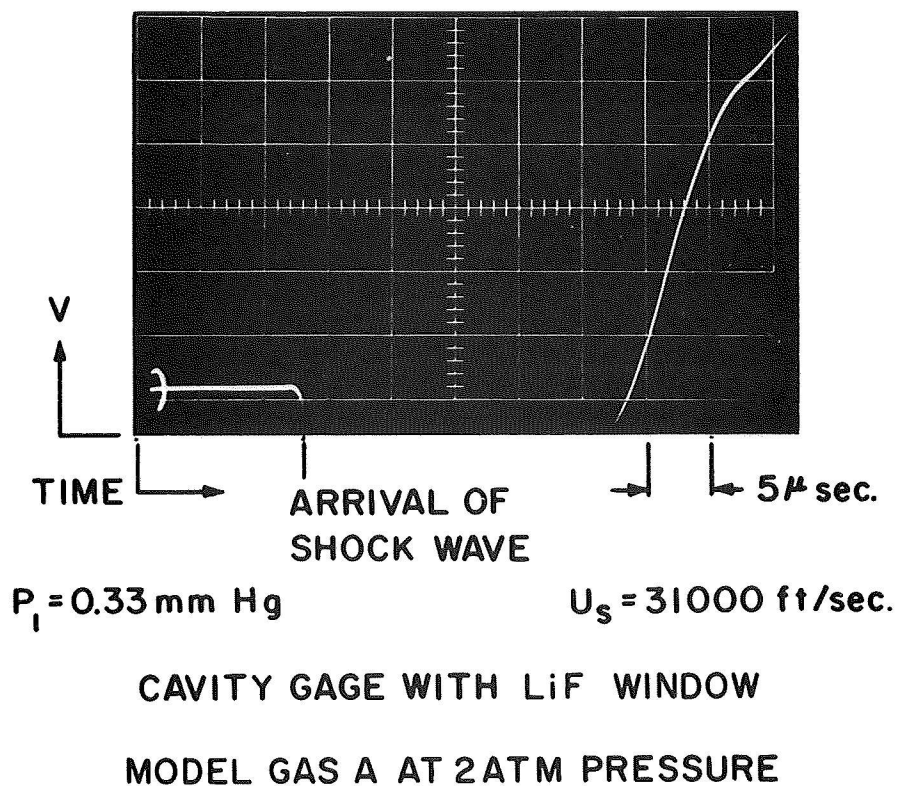
Figure 3.17 - Oscilloscope traces of cavity gage response with LiF window shows strong photoelectric effect when model filled with argon.
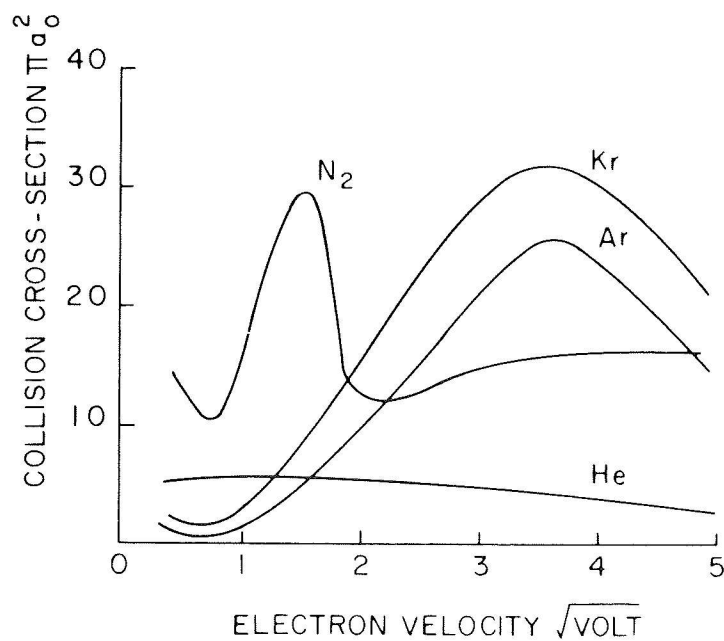
Figure 3.18 - Total collision cross-sections of several gases for electrons with various energies.

Figure 3.19 - Oscilloscope trace of cavity gage response with LiF window. Model filled with 50% Kr - 50% He gas mixture.
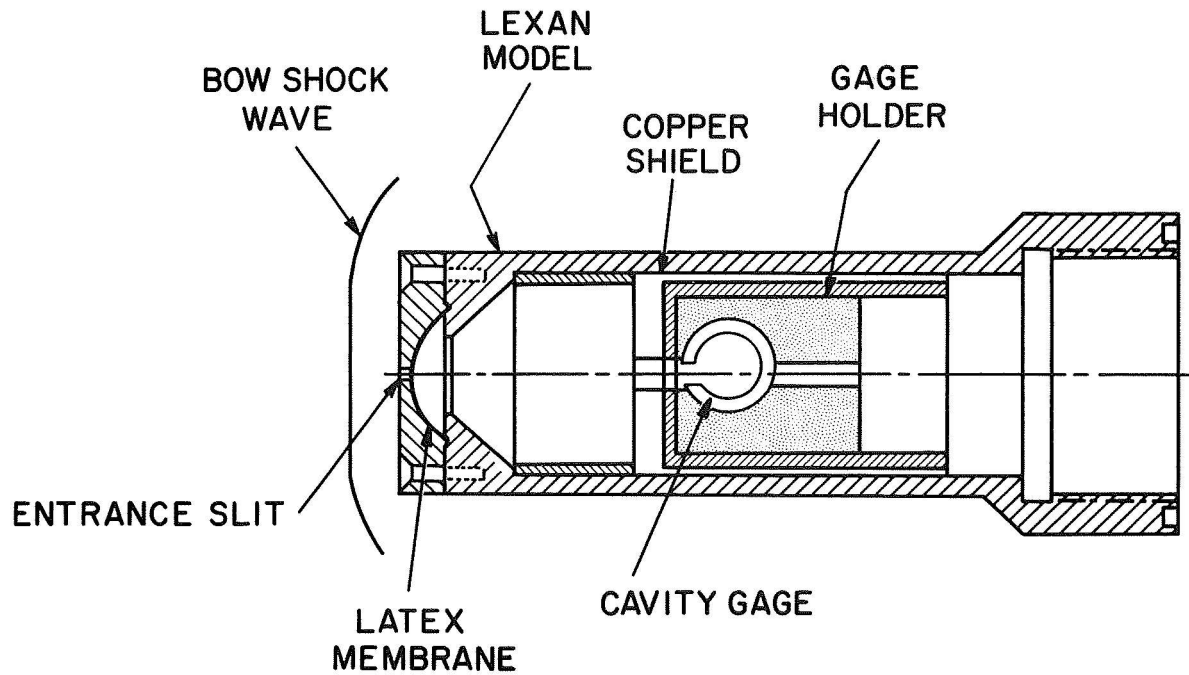
Figure 3.20 - Windowless cavity gage - model system.
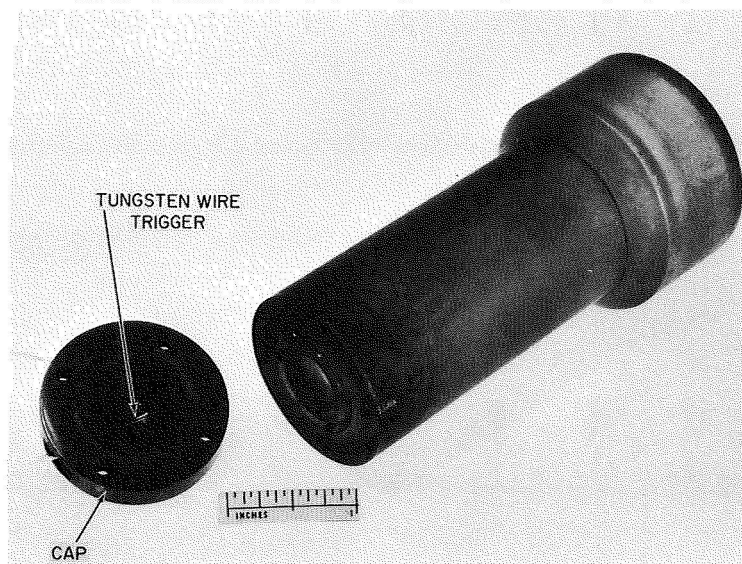
Figure 3.21 - Photograph of the cylindrical, windowless model. Arrow indicates the wire used for rupturing latex membrane.

ENTRANCE SLIT

LEADS FOR TUNGSTEN
WIRE TRIGGER

INCHES
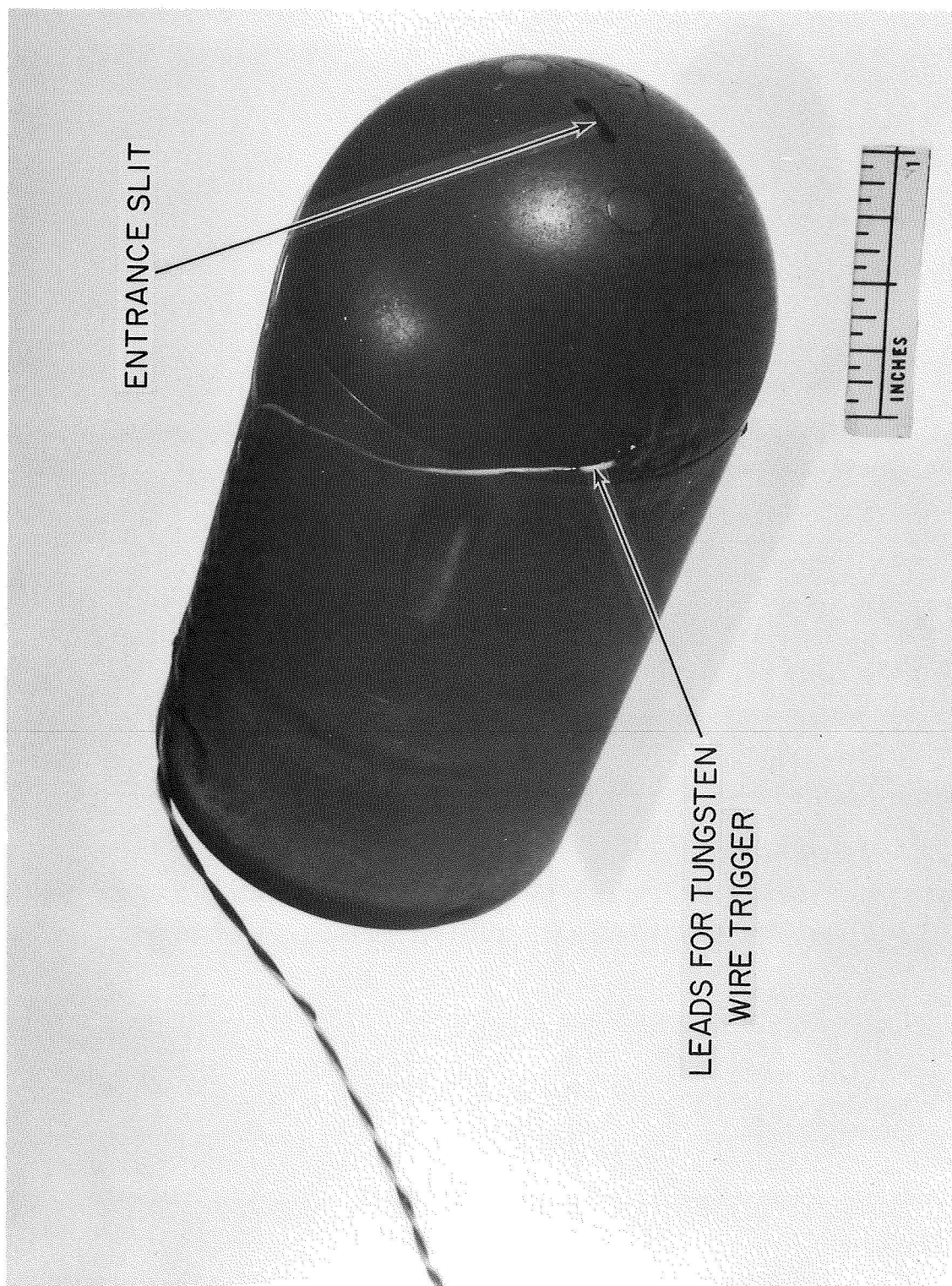
Figure 3.22 - Photograph of the hemispherical windowless model.
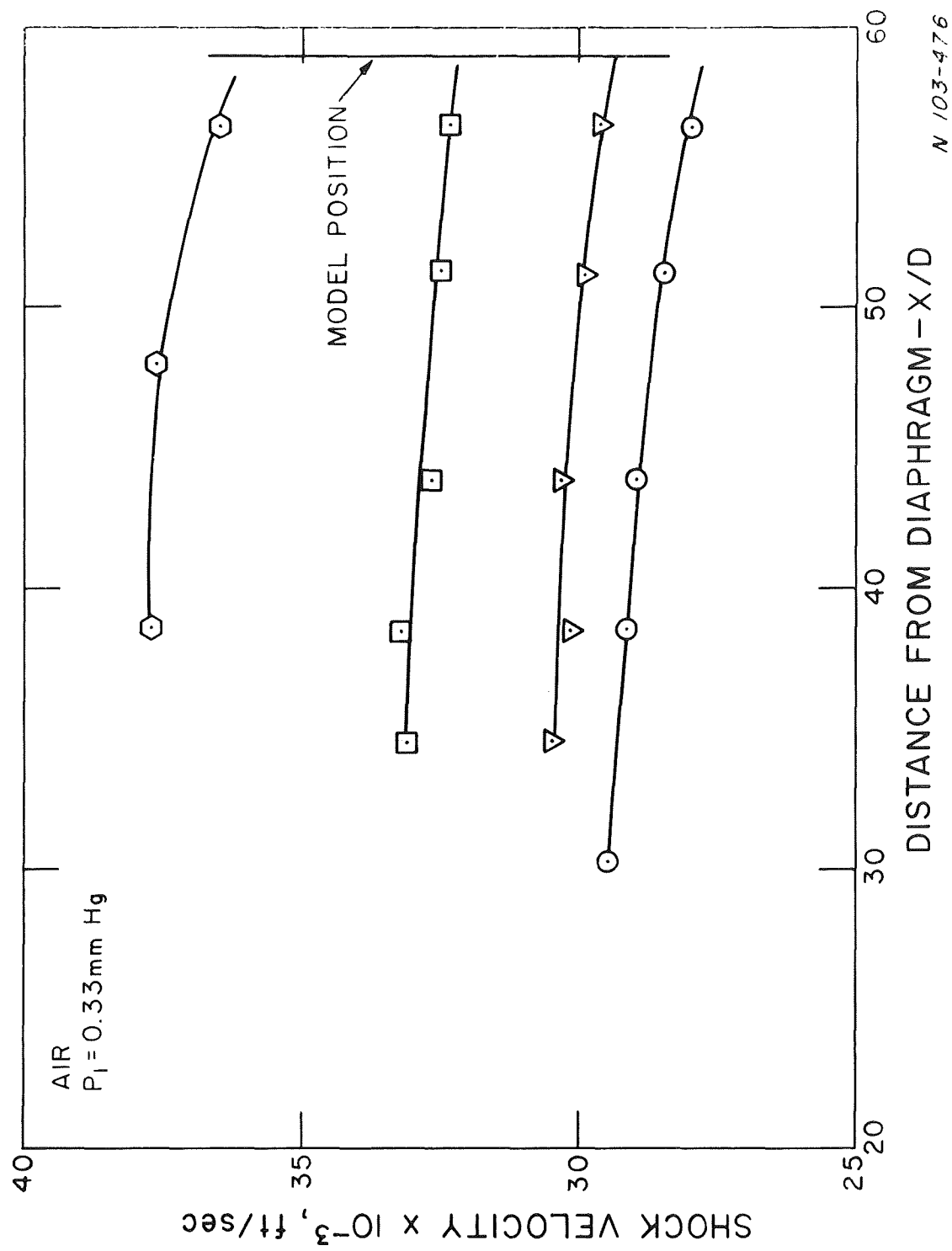
Figure 4.1 – Shock velocity variation along the length of the shock tube.

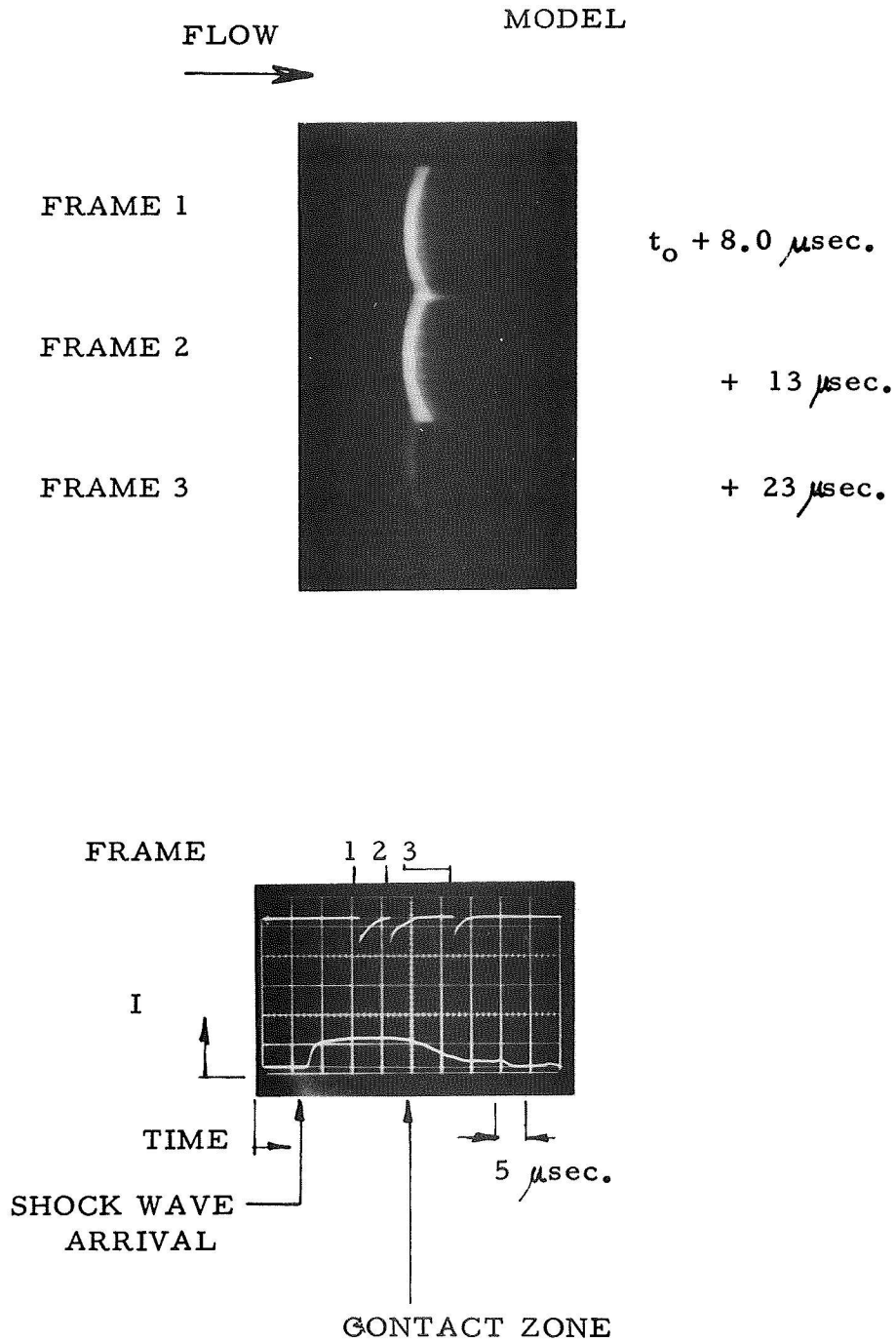N 103-476
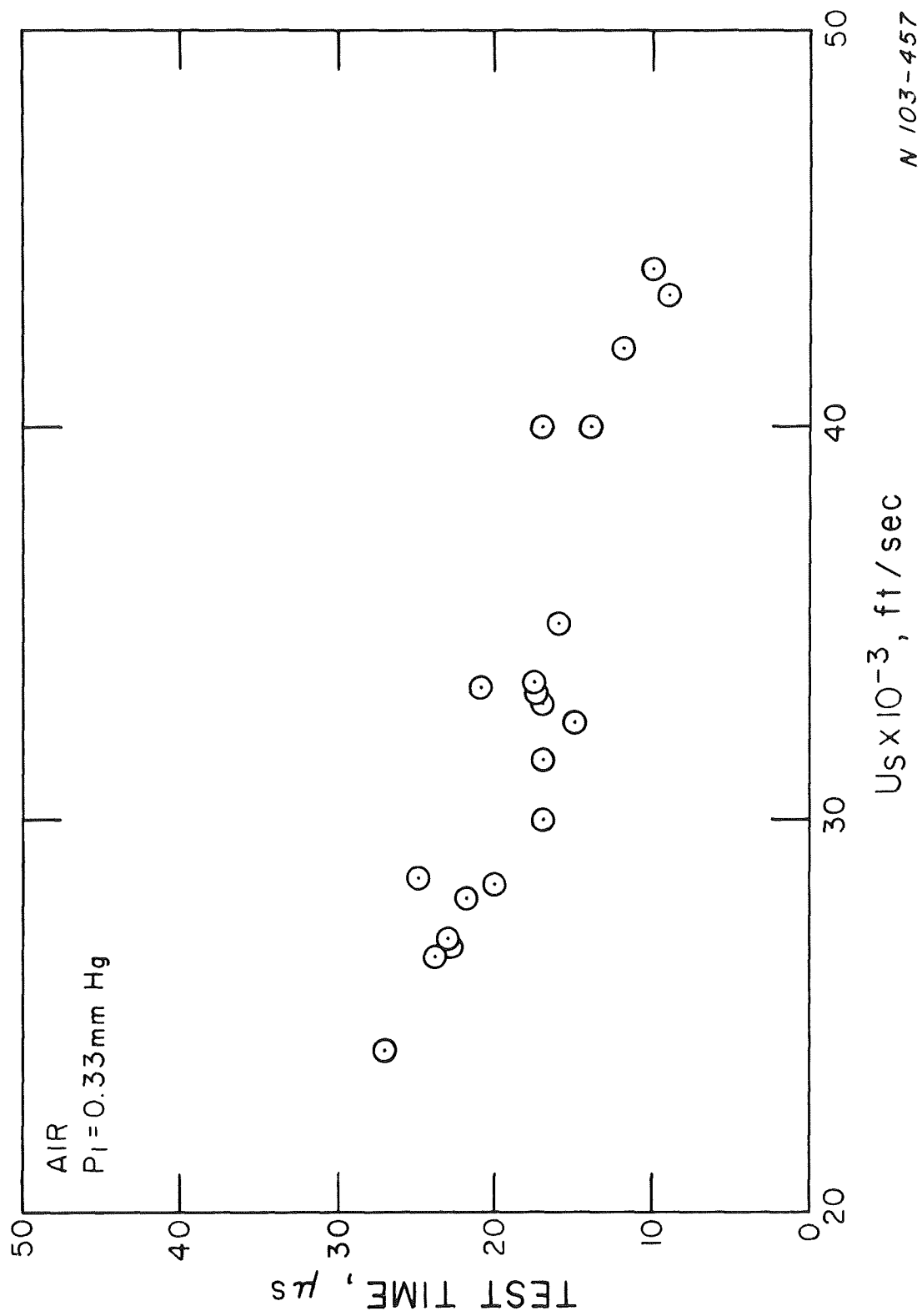
Figure 4.2 - Test time as a function of shock velocity.

AIR
$P_1 = 0.33$mm Hg

$Us \times 10^{-3}$, ft/sec

TEST TIME, μs

N 103-457

FLOW MODEL

FRAME 1

$t_o + 8.0$ μsec.

FRAME 2

$+ 13$ μsec.

FRAME 3

$+ 23$ μsec.

FRAME   1 2 3

I

TIME

SHOCK WAVE
ARRIVAL

5 μsec.

CONTACT ZONE

Figure 4. 3 - Image converter camera photographs of stagnation region shock
layer on a hemispherical model. Lower photograph shows signal
from camera monitor and response of photomultiplier viewing
stagnation region flow from sidewall. The incident shock velocity
and initial tube pressure were 28,500 ft/sec and 0.33 torr re-
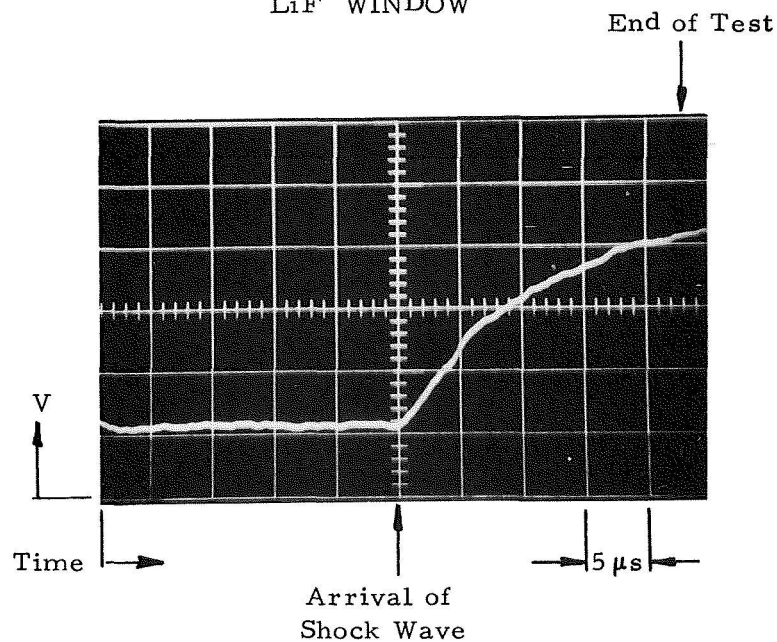spectively.
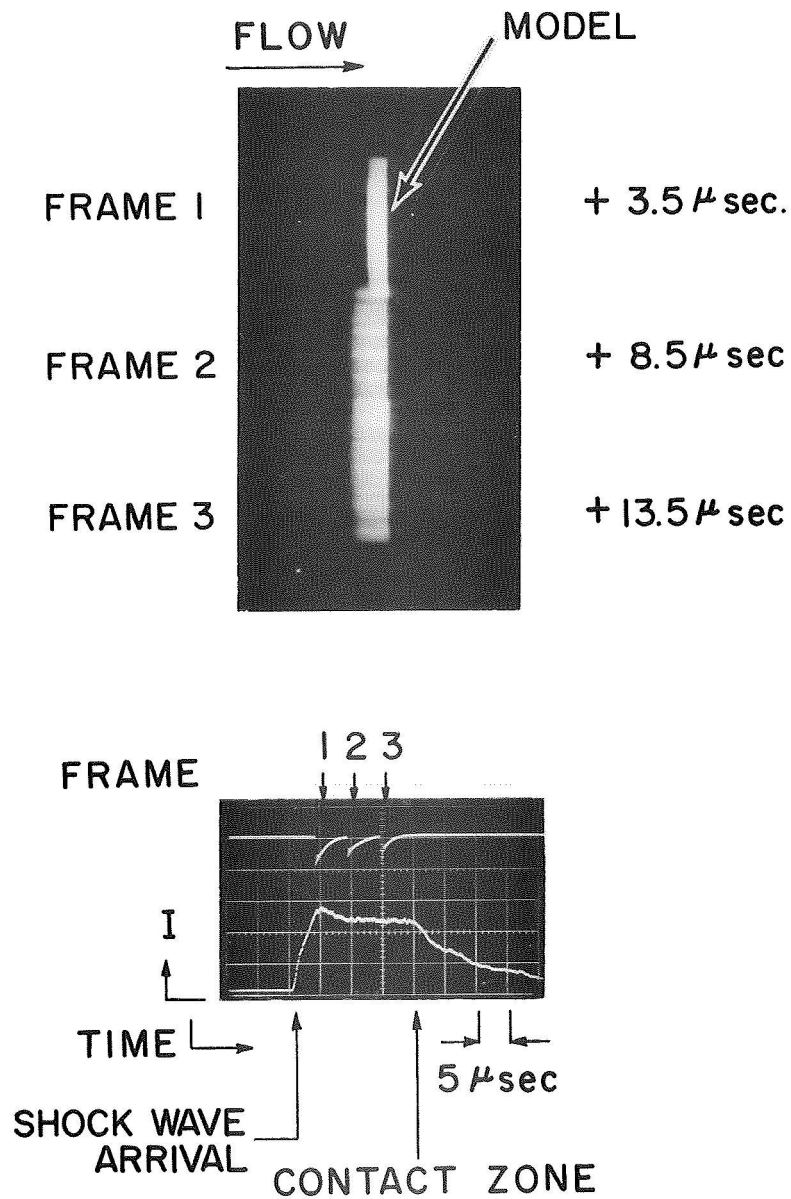
Figure 4.4 - Image converter camera photographs of stagnation region shock layer of a cylindrical model taken from sidewall. Lower photograph shows signal from camera monitor and response of photomultiplier viewing stagnation region flow from sidewall. The incident shock velocity and initial tube pressure were 28,500 ft/sec and 0.33 torr respectively.

QUARTZ WINDOW

End of Test

V

Time

Arrival of
Shock Wave

5 μs
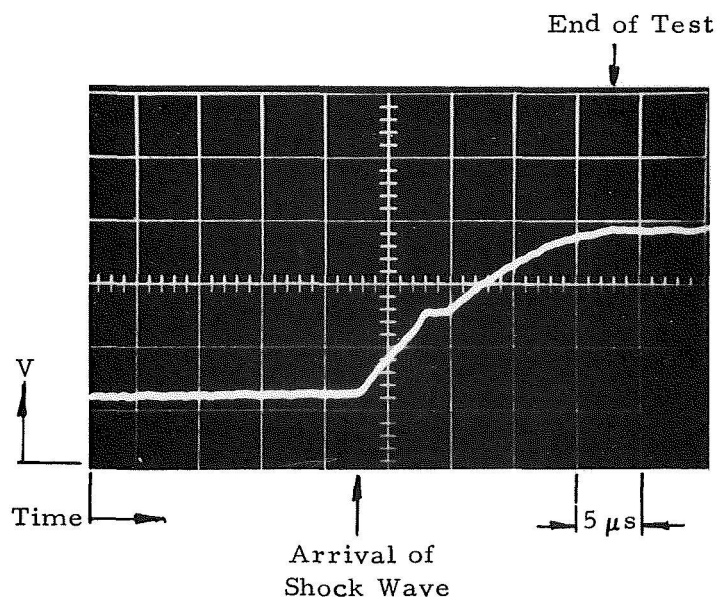
P_1 = 0. 33 mm Hg U_s = 31,600 ft/sec

LiF WINDOW

End of Test

V

Time

Arrival of
Shock Wave

5 μs

P_1 = 0. 33 mm Hg U_s = 29,000 ft/sec

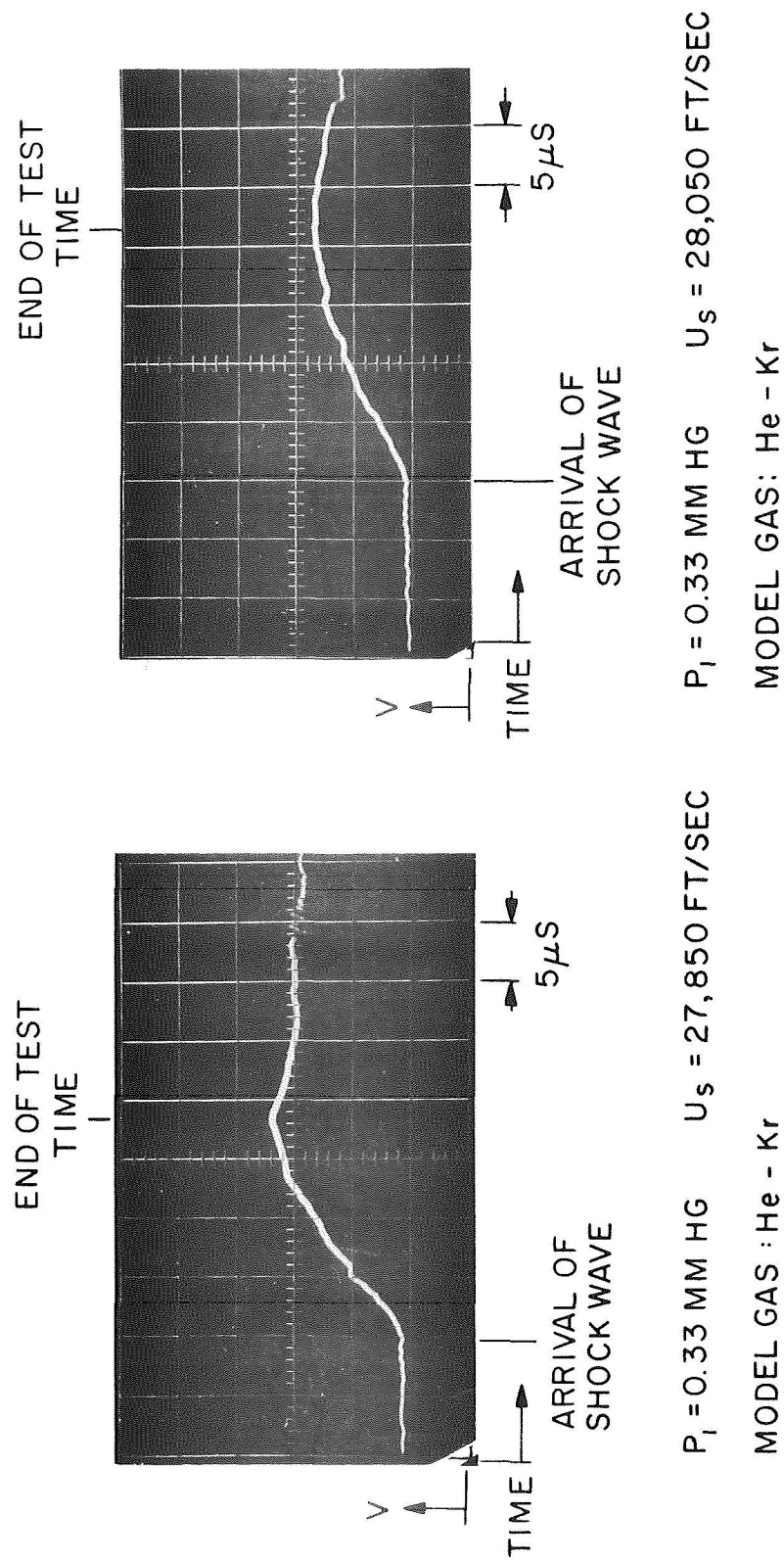Figure 4.5 - Oscilloscope traces of cavity gage response with quartz and LiF
windows.

Figure 4.6 - Oscilloscope traces obtained with the windowless gage system.
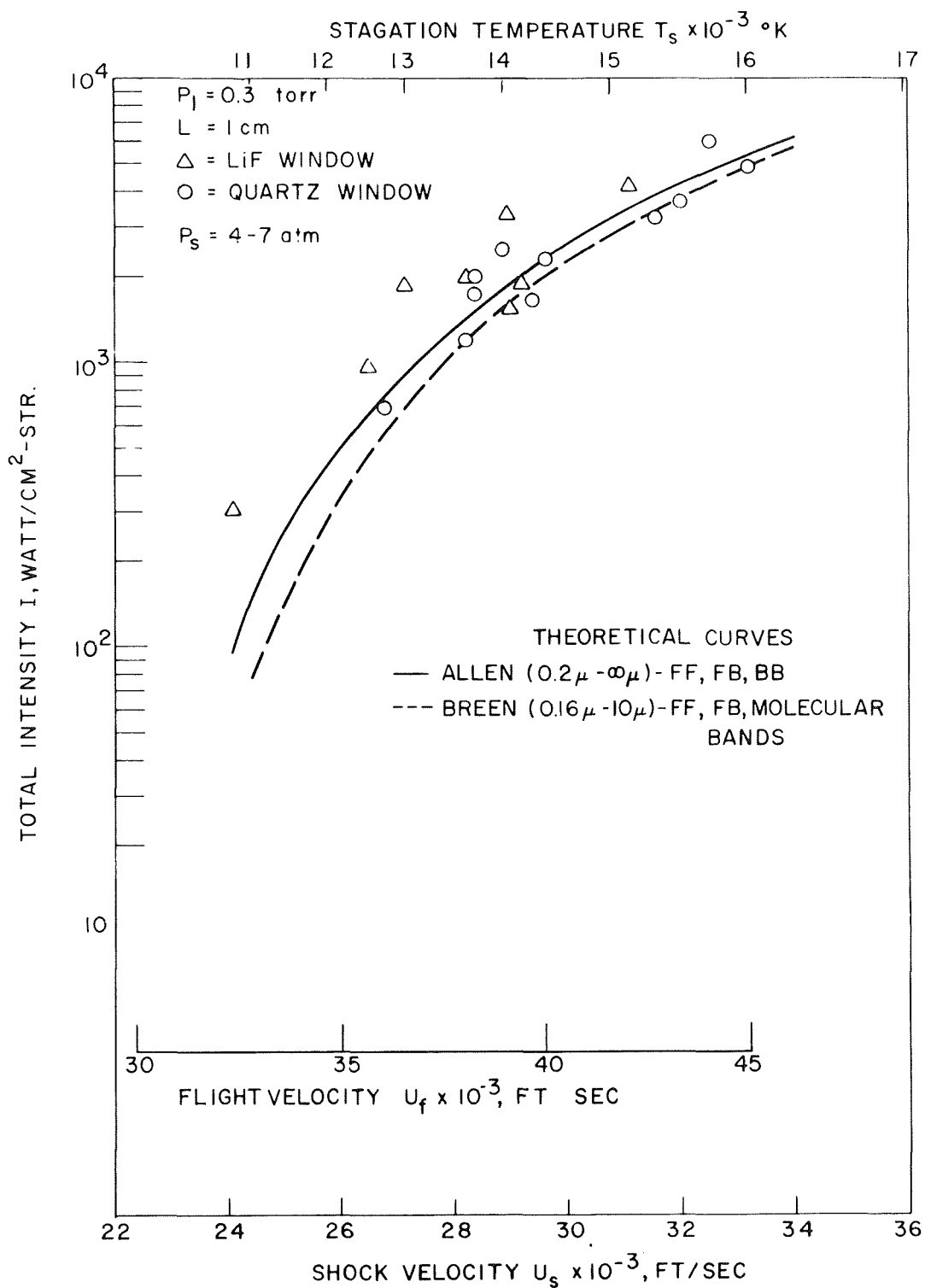
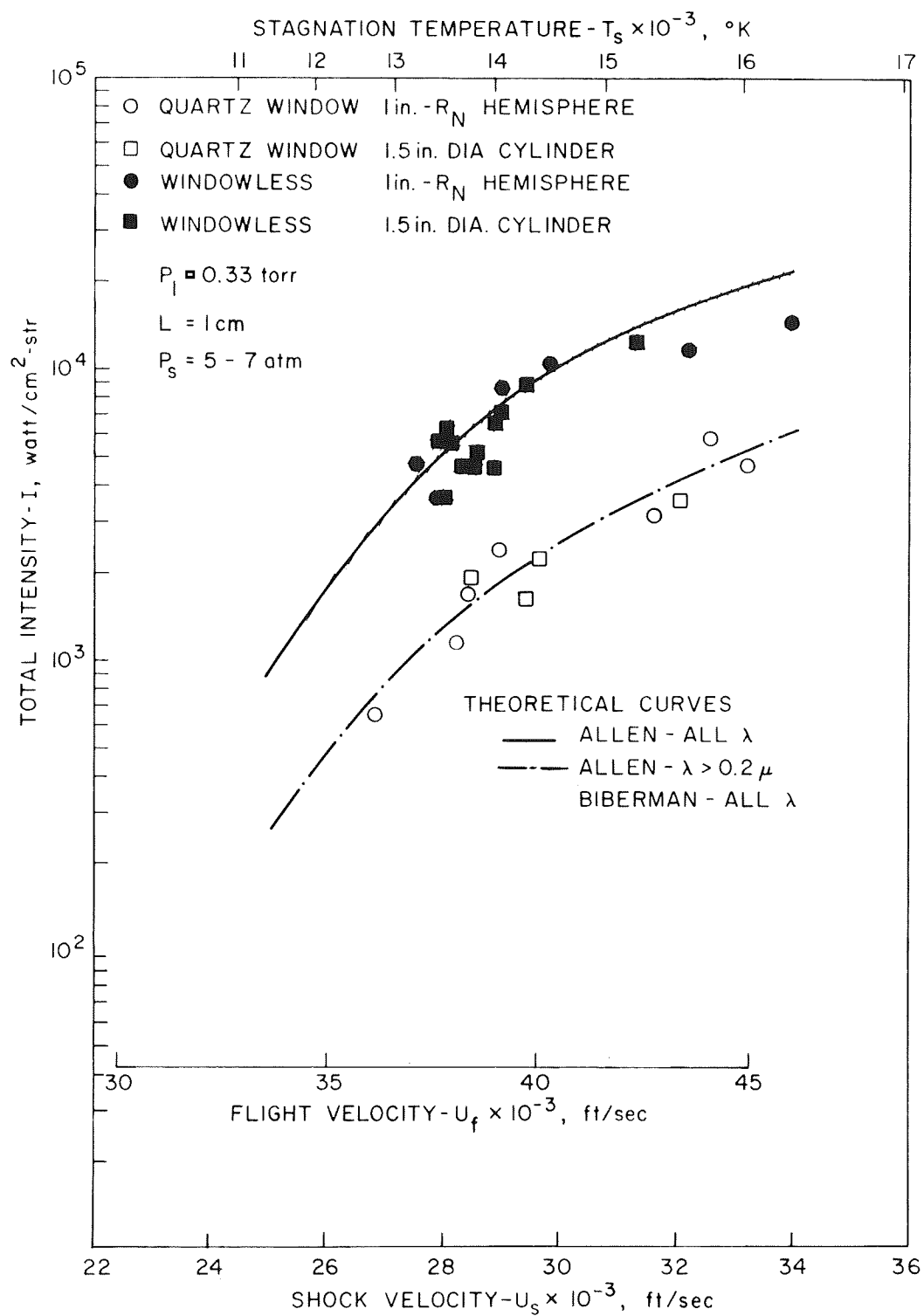Figure 5.1 - Comparison of experimental data for quartz and lithium fluoride windows.

Figure 5.2 – Comparison of experiment and theory for window and windowless gage-model configurations.